The mechanical properties of a surface-modified layer on poly(dimethylsiloxane)

K. L. Mills[1], Xiaoyue Zhu[2], Shuichi Takayama[2,4], and M. D. Thouless[1,3]

[1]Department of Mechanical Engineering, University of Michigan, Ann Arbor, MI, 48109, USA
[2]Department of Biomedical Engineering, University of Michigan, Ann Arbor, MI, 48109, USA
[3]Department of Materials Science & Engineering, University of Michigan, Ann Arbor, MI, 48109, USA
[4]Macromolecular Science and Engineering Program, University of Michigan, Ann Arbor, MI, 48109, USA

Abstract

Surface-modification of the elastomer poly(dimethylsiloxane) by exposure to oxygen plasma for four minutes creates a thin, stiff film. In this study, the thickness and mechanical properties of this surface-modified layer were determined. Using the phase image capabilities of a tapping-mode atomic-force microscope, the surface-modified region was distinguished from the bulk PDMS; specifically, it suggested a graded surface layer to a depth of about 200 nm. Load-displacement data for elastic indentation using a compliant AFM cantilever was analyzed as a plate bending on an elastic foundation to determine the elastic modulus of the surface (37 MPa). An applied uniaxial strain generated a series of parallel nano-cracks with spacing on the order of a few microns. Numerical analyses of this cracking phenomenon showed that the depth of these cracks was in the range of 300–600 nm and that the surface layer was extremely brittle, with its toughness in the range of 0.1–0.3 J/m^2.

1 Introduction

Polydimethylsiloxane (PDMS), a clear elastomer, is a very common material used in a myriad of applications in bioengineering, electronics, and MEMS. Specifically, some of these applications include micromachined mechanical and chemical sensors [1], stamp material for soft lithography [2, 3], and microfluidics devices [4-6]. PDMS is widely used because it is biologically inert, gas permeable, an insulator, and good for rapid prototyping of devices. However, for applications where laminar flow or wetting of fluids is desired, the inherent hydrophobicity of the PDMS surface is not ideal. Therefore, the surface of PDMS is often made hydrophilic by oxidation techniques which emulate environmental exposure [7, 8], only in an expedited manner. In addition to changing the surface chemistry, oxidation creates a stiff, thin surface-modified layer [9-11]. The oxidized PDMS exhibits mechanical behaviors that are characteristic of elastically-mismatched layered materials, but at the nano-scale. Specifically, moderate uniaxial tensile strains (for an elastomer) produce periodic parallel cracks in the stiff surface-modified layer [12], and compressive strains induce surface buckling [9].

This behavior has proved to be useful for applications for which patterns at a nano-scale are desired. For example, a recent study showed that when the nano-cracks in the surface-modified layer of oxidized PDMS are decorated with adhesive proteins, they can support the growth and modulation of cells [12]. Additionally, nano-crack patterning has been used as the platform for creating reconfigurable nano-channels [13]. For these applications it would be particularly advantageous to be able to design patterns of nano-cracks and to understand how the patterns would respond to applied strains. The basic framework for such design methodologies is provided by the traditional tools of thin-film mechanics. However, this requires knowledge of the mechanical properties of the layered system, including the elastic properties and toughness of

both the surface-modified layer and the substrate, and the thickness of the surface-modified layer. While the bulk material (the PDMS substrate) can be easily characterized using standard tests, the surface-modified layer is too thin for its properties to be measured directly. As a result, there is a significant challenge in determining the properties of the surface-modified layer on PDMS.

Previous work has indicated that a surface-modified layer created by plasma oxidation or by exposure to ultraviolet/ozone radiation is less than a micron thick and can have an elastic modulus of anywhere between 4 and 750 MPa [9-11, 14]. Two different techniques have been used to measure the thickness of the surface-modified layer. First, a scanning electron microscope was used to image the cross-section of PDMS that had been exposed to plasma oxygen for 15 minutes [9]. A demarcation between two regions was observed approximately 0.5 μm below the free surface, and this was taken to be the depth of the surface-modified layer. Second, a combination of neutron reflectometry and X-ray photoelectron spectroscopy was used to show that the thickness of the surface-modified layer decreased from 160 nm after 80 seconds of exposure to oxygen plasma, to 130 nm after 180 seconds of exposure [11].

Estimates of the elastic modulus of the surface-modified layer include those calculated from the buckling wavelength of a compressed surface-modified layer and those calculated from nanoindentation results. When a stiff layer buckles on an elastic foundation there is a characteristic wavelength that depends on the modulus and thickness of the layer and on the modulus of the substrate. Having estimated the layer thickness associated with 15 minutes of plasma oxidation, Bowden *et al.* [9] used this result to estimate the elastic modulus of the surface layer to be about 750 MPa. Nanoindentation analyses based on indentation curves generated with the atomic force microscope have produced estimates for the stiffness of surface-modified

layers created using ultraviolet/ozone radiation for periods up to 90 minutes. The values of these estimates are 4–11.2 MPa [14] and 15–87 MPa [10]. However, the limitations of using indentation techniques to measure the modulus are well recognized when a stiff layer is on top of a compliant substrate, as the indentation is affected by the substrate over the full range of indentation depths [15, 16].

In this paper, an investigation of the material properties of plasma-oxidized PDMS is presented—an integral aspect of understanding the mechanics of nano-cracking in this system. The properties of the PDMS are straightforward to determine with established experimental methods and are presented in Section 2. Addressing the challenge of assessing the material properties of the surface-modified layer, Section 3 demonstrates a two-step method, using the atomic-force microscope, to determine its thickness and elastic modulus. If different oxidizing conditions were to be explored, it is envisioned that this method would be a relatively quick and easy technique to assess the properties of the resulting surface-modified layer. Finally, in Section 4 the fracture behavior of a surface-modified layer is discussed in the light of the measured material properties.

2 Materials preparation and properties of the bulk PDMS

2.1 Materials preparation

Initial studies showed that both the ratio of the polymer to the curing agent and the curing schedule affected the constitutive behavior of the resulting elastomer. Therefore, care was taken to ensure that all experiments were performed with PDMS that was produced using the same mixing and curing parameters. In particular, Dow Corning (Sylgard 184) PDMS was prepared with a ratio of 10 parts of polymer to 1 part of curing agent. The liquid polymer was poured into

glass Petri dishes and then cured at 60°C for three hours followed by 12 hours at 150°C. The resulting thickness of the PDMS sheets used throughout this study was 2.0 ± 0.2 mm.

The PDMS was oxidized by exposing the cured sheets to oxygen plasma in the Pyrex chamber of a plasma etcher.[1] A maximum power of 100 W was used for a period of four minutes with a pure oxygen environment at a relative vacuum of about 300 mtorr. However, precise control of the oxidation conditions could not be guaranteed between different oxidation runs. Furthermore, there was evidence of some variation in the effects of the oxidation across a specimen in a single run. In the results that follow, it will be indicated when comparisons are being made between specimens oxidized together or in separate runs.

2.2 Constitutive properties of the bulk PDMS

The constitutive behavior of the PDMS was measured with tensile tests. Tensile specimens were sliced from the cured sheets of PDMS in the dog-bone shape of dimensions shown in Fig. 1. An initial gage length of 18.5 mm was drawn on the specimen, and the specimen was clamped in wedge grips. The tensile tests were performed at a constant displacement rate of 1 mm/sec, and the load was measured using a 250 N load cell. The nominal stress was calculated as the load divided by the original cross-sectional area. A CCD optical camera was used to capture images of the deformed gage length at regular intervals throughout the experiment. These images were used to compute the nominal strains.

A typical nominal stress-strain curve obtained from the PDMS tensile experiments is shown in Fig. 2. Although the stress-strain curve was sensitive to the curing conditions, it was very reproducible for a given set of conditions. The behavior of the elastomer was non-linear

[1] SPI Supplies, Plasma Prep II

elastic; no hysteresis could be detected upon cyclic loading. Although the curve is non-linear, there is an initial linear portion up to about 30–40% strain. The linear-elastic modulus in this regime was determined to be 3.5 ± 0.2 MPa. The tensile tests were repeated for specimens of the cured PDMS stored for prolonged periods at ambient conditions (in a laboratory, away from direct sunlight) and for specimens of the cured PDMS subjected to the four-minute oxidation treatment. The nominal stress-strain curves for all samples were identical, except for the oxidized samples where there was a slight decrease in the average failure strain from about 80% to about 70%. It is clear that the surface-modified layer was sufficiently limited in its extent that it did not affect the macroscopic properties beyond the slight decrease in failure strain, and the cured PDMS was very stable.

2.3 Fracture properties of the bulk PDMS

Trouser specimens were sliced from the 2 mm-thick sheets of PDMS with an overall width of 20 mm and leg length of 40 mm (Fig. 3a). The surface of the PDMS was scored along the projected crack path with a razor blade to ensure that the crack grew in the center of the legs and fracture remained as a tearing mode, deterred from transitioning to an opening mode. The specimens were loaded at a fixed displacement rate of 1 mm/sec (Fig. 3b). The load required to tear the PDMS, F_t, was monitored throughout the test and remained constant at 0.3 ± 0.01 N during steady-state crack growth. From this tear load and the thickness, t, of the fractured surface (1.8 ± 0.2 mm), the mode-III toughness was calculated as $\Gamma_{III} = 330 \pm 27$ J/m^2 from the relationship $\Gamma_{III} = 2F_t / t$.

Compact tension specimens were prepared according to ASTM Standard D5045–99 (Fig. 4). The specimens were loaded at the pin points and a CCD camera was used to monitor

the crack growth during the tests. Examples of the resulting load versus displacement curves are shown in Fig. 5. The fracture toughness, K_{Ic}, was calculated from the failure load as defined in the standard. The mode-I toughness was then determined to be $\Gamma_I = 238 \pm 50$ J/m^2 from the relationship $\Gamma_I = (1-\nu^2)K_{Ic}{}^2 / E$, with $E = 3.5 \pm 0.2$ MPa and $\nu = 0.5$ (as appropriate for an elastomer). The values of the mode-III toughness and the mode-I toughness appear to be reasonably consistent, and they will be used as a point of comparison when investigating fracture of the surface-modified layer in a subsequent section of this paper.

3 Properties of the surface-modified layer

3.1 Thickness of the surface-modified layer

Imaging a cross-sectioned piece of oxidized PDMS is the most obvious approach to measure the thickness of the surface-modified layer. However, it was found that sectioning the PDMS by means of a scalpel blade or by fracture created a fracture lip at the free surface. This feature was at a similar scale (~0.5 μm) to the expected thickness of the surface-modified layer and dominated any observations made in the scanning electron microscope or atomic-force microscope. It was found that this problem could be eliminated by bonding two slabs of oxidized PDMS and then fracturing the bonded specimen to expose a cross-section containing the interface. An oxidized surface of PDMS readily forms a permanent bond upon contact with another oxidized surface of PDMS, a fact that is exploited in the manufacture of micro-fluidic devices [17]. However, for the bond to form, at least one of the oxidized surfaces must retain sufficient compliance to achieve good conformal contact. In particular, the surface of PDMS that had been oxidized for four minutes, which was the focus of this study, did not have sufficient compliance. However, oxidation for only one minute appeared to provide the required change in surface chemistry, while retaining sufficient compliance. Therefore, for the purposes

of this study, PDMS that had been oxidized for four minutes was bonded to PDMS slabs that had been oxidized for one minute. A crack was then introduced into one of the back surfaces (perpendicular to the bonded interface), and the specimen was cleaved. The resultant fracture surface was relatively flat, with no delamination or fracture features at the interface.

Imaging a fractured section optically or in an environmental scanning electron microscope produced no contrast between the surface-modified layer and the bulk PDMS used in this study. Nor were any topographical features identifiable at the bonded interface using the atomic-force microscope[2] (AFM). However, a clear interface was observed using the phase-imaging function of the AFM in tapping mode. The phase image is a three-dimensional representation of the phase lag between the tapping-mode cantilever's oscillations and the input signal. The phase lag has been shown to depend on the elastic modulus as well as other properties (*e.g.*, visco-elasticity and adhesion) of the material being profiled [18-21]. Therefore, the fact that a contrast in the phase image at the bonded interface could be seen was taken to be an indication that there was a local change in the material properties at the oxidized surface. The distance over which this contrast could be detected was taken to be a measure of the thickness of the surface-modified layer.

A phase image of the cross-section near the interface region is shown in Fig. 6a. In this image a clear demarcation can be seen between the PDMS oxidized for one minute (on the left) and the PDMS oxidized for four minutes (on the right). The phase image did not seem to be very sensitive to any of the minor topographical features captured in a height image of the same region (Fig. 6b). A line trace on the phase image across the interface is shown in Fig. 6c. This trace indicates that any compositional changes within the surface-modified layer were not

[2] MultiMode Scanning Probe Microscope, Veeco Instruments, Inc.

uniform. The lowest point of the line trace was taken to be the bond line between the two oxidized samples, and the distance to where the phase angle returned to the average bulk value was taken to be the surface-modified layer thickness. Therefore, the changes are a maximum at the surface and decay to the bulk values over a few hundred nanometers.

The absence of any discontinuity in the phase angle at the interface region in Fig. 6c indicates that the two surfaces (for the PDMS oxidized for one minute and for the PDMS oxidized for four minutes) may have similar compositions. The only difference between the two oxidation treatments appears to be the thickness of the surface-modified layer. The surface-modified layer for the specimen oxidized for only one minute appeared to be significantly thinner than the layer resulting from oxidation for four times as long. Measurements were taken from two sets of bonded specimens, and multiple traces were taken from each of these specimens. These measurements indicated that the thickness of the surface-modified layer of the specimens oxidized for four minutes was 200 ± 40 nm, with the full range of uncertainty being exhibited in a single specimen. The measurements also indicated that the thickness of the surface-modified layer in a specimen oxidized for one minute was approximately half as thick as a layer resulting from four minutes of oxidation. Associated experiments in which both halves were oxidized for only one minute confirmed that one minute of oxidation indeed resulted in a surface-modified layer thickness of 110–125 nm [22]. This result is suggestive of a diffusion-dominated oxidation process where the depth is predicted to be proportional to the square-root of the time of exposure. Although the data does not allow the issue to be resolved unambiguously, the relationship between the phase angle and the distance from the presumed interface shown in Fig. 6c is not inconsistent with an error function that would be expected to result from a diffusion-dominated process. However, for the purposes of the subsequent analyses, an

approximation was made that the properties of the surface-modified layer followed a linear profile.

3.2 Elastic modulus of the surface-modified layer

Nanoindentation was performed using the "force mode" of the AFM. Before each set of indents was performed, the cantilever deflection was calibrated by bringing the probe into contact with silicon, which provided a hard reference surface. The first set of experiments involved the use of a relatively stiff AFM probe (with a cantilever stiffness of $k = 40$ N/m, as determined by the manufacturer[3]) to indent oxidized PDMS. Figure 7 shows that the resultant plot of load against indentation depth is reminiscent of a characteristic plastic indent [23]. The indentation depth reached between 2 and 3 μm, and subsequent imaging in the AFM revealed a puncture in the surface-modified layer measuring about 1 μm in width and 50 nm in depth. However, rather than trying to extract any information about the surface-modified layer from this type of behavior, the effect of using a more compliant cantilever was explored.

Qualitatively different indentation curves were obtained when a relatively compliant cantilever ($k = 0.58$ N/m) was used to indent unoxidized and oxidized PDMS surfaces. Indentation on an unoxidized PDMS surface showed the classical non-linear behavior (with essentially no hysteresis) associated with the contact mechanics of elastic indentation (Fig. 8). No permanent indentation impression was found during subsequent imaging by AFM. In contrast, indentation on an oxidized PDMS surface resulted in a linear relationship between the cantilever deflection and the translation of the sample, with some evidence of adhesive contact as the AFM probe came into contact with and left the surface (Fig. 9). Multiple indentations were performed on a single sample of PDMS that had been oxidized for four minutes, with

[3] Veeco Probes, Inc.

recalibration repeated during the experiment. All the indentations were very consistent and resulted in a characteristic plot of load against indentation depth shown in Fig. 10.

This linear relationship between load and indentation depth for the oxidized PDMS indicates that the contact area between the probe tip and the material did not increase with indentation depth, as would be expected from classical indentation models. Instead, the behavior is consistent with point loading of an elastic beam on an elastic foundation. It is this model that can be used to extract the properties of the surface-modified layer. The deflection, Δz_i, of an elastic plate bonded to an elastic half-space and subjected to a point load, P, is given by [24]

$$\Delta z_i = \frac{P}{3\sqrt{3}}\left(\frac{(1+\nu_s)^2(3-4\nu_s)}{4E_s^2(1-\nu_s)^2 D}\right)^{1/3}, \qquad (1)$$

where D is the bending stiffness of the plate, E_s is the modulus of the substrate and ν_s is the Poisson's ratio of the substrate. As discussed in Section 2, E_s for this material is 3.5 ± 0.2 MPa, and ν_s can be taken to be equal to 0.5. Therefore, the relationship between the indentation depth and applied load is given by

$$\frac{P}{\Delta z_i} = 9.1(\pm 0.3)\times 10^4 D^{1/3} \qquad \text{N/m.} \qquad (2)$$

From Fig. 10, it can be seen that the experimental relationship between the load and indentation depth is in the range of 1.9 to 2.1 N/m. Therefore, a comparison with Eqn. 2 indicates that the bending stiffness of the surface layer is equal to (1.1 ± 0.2) x 10^{-14} N.m.

To estimate the modulus from a bending stiffness requires knowledge of the thickness and whether the modulus varies through the thickness of the surface-modified layer. As discussed in Section 3.1, it is assumed for the purposes of analysis that the modulus decreases

linearly from a value designated as E_f at the surface to E_s at the depth previously identified as the thickness of the surface-modified layer, h. With this linear assumption, the bending stiffness of the surface layer can be calculated as

$$D = \frac{\left(\overline{E}_f^{\,2} + 4\overline{E}_f\overline{E}_s + \overline{E}_s^{\,2}\right)h^3}{36(\overline{E}_f + \overline{E}_s)}. \tag{3}$$

Here, $\bar{E}_f$ and $\bar{E}_s$ refer to the plane-strain moduli of the surface-modified layer and PDMS, respectively. Substituting into this equation the values $h = 200 \pm 40$ nm, $E_s = 3.5 \pm 0.2$ MPa, $\nu_s = 0.5$, and $D = (1.1 \pm 0.2)$ x 10^{-14} N.m results in a value for the surface modulus of $\bar{E}_f = 37 \pm 10$ MPa. This maximum value of the modulus at the surface of the oxidized layer is between 7 and 13 times larger than the modulus of the substrate. If it were to be assumed that the properties of the surface-modified layer were not graded, but were uniform over a thickness of about 200 nm, then the effective modulus of the layer would be 12 ± 3 MPa from the relationship $D = Eh^3/12(1-\nu^2)$.

In the experiments described in the following section, buckling of the surface layer was observed. The details of this observation can be used as a point of comparison for the results presented above. For a uniform plate of thickness h, the buckling wavelength of a surface layer is expected to be of the form [25, 26].

$$\lambda = 9.97\left(D\left(1-\nu^2\right)/E_s\right)^{1/3} \tag{4}$$

For the parameters determined in the present study this equation indicates that the buckling wavelength would be about 1.3 μm. The effect of a graded layer on the buckling wavelength is being studied [27]; nevertheless, this result is very close to the observed wavelength which was

found to be 1.34 ± 0.06 μm and provides some confirmation of the magnitude of the properties of the surface-modified layer.

4 Fracture of the surface-modified layer

4.1 Experimental observations

Once the properties of the surface-modified layer have been determined, observations of the nano-cracking behavior can be compared to mechanics models. A controlled experiment was performed in order to study the behavior of the nano-cracking with respect to applied tensile strain. Several PDMS specimens were oxidized for four minutes in the same run in order to ensure that the surface-modified layer on each was as close to the same as possible. After oxidation, some of these specimens were used to determine the resulting thickness and modulus of the surface-modified layer (as reported in the previous sections). The remaining rectangular pieces (40 mm x 10 mm x 2 mm) were individually mounted in a manual micrometer-screw-driven tensile machine[4] and strained in tension. These specimens were organized into five sets of two specimens, and each set was tested to different levels of nominal strain: 6, 10, 15, 20, and 30%. One specimen from each set was removed from the testing machine and relaxed before being examined. The other specimen from each set was left in place under an applied strain while a PDMS replica was created of its surface. To ensure complete removal of the replica the cracked surface was first exposed to a silane treatment[5] to increase the hydrophobicity of the surface-modified PDMS. Square sections of approximately 10 mm by 10 mm were then cut from the center region (away from the ends gripped by the stretcher) of both the relaxed

[4] MicroVice Holder (S.T. Japan USA, LLC. FL, USA)

[5] For seven minutes in a vacuum chamber a 1:1 mixture of (tridecafluoro-1,1,2,2-tetrahydrooctyl)-1-trichlorosilane and mineral oil was evaporated onto the cracked surface to form a monolayer of silane molecules.

specimens and the replicas of the strained surfaces. The surfaces of both sets of specimens were imaged using the AFM in tapping mode.

The applied tensile strain resulted in a series of parallel nano-cracks in the surface-modified layer oriented perpendicular to the direction of stretching. The average crack spacing was measured from a series of AFM images and is plotted as a function of the applied strain for all the specimens in Fig. 11. Consistent with prior analyses and observations of thin-film cracking [28-30], the average crack spacing decreased with increasing applied strain. In addition to the nano-cracks, for tensile strains of 15% and above, surface buckles were induced perpendicular to the cracks with a wavelength of 1.34 ± 0.06 μm. An image taken with the AFM of a surface that has been cracked by an applied strain and then allowed to relax is shown in Fig. 12; while an image taken from a replica of a strained surface with the accompanying surface buckling is shown in Fig. 13.

The buckles created by the application of the tensile strain seem to be created by a different mechanism than those created by an imposed compressive strain [9]. The surface buckles are always observed to occur at strains greater than those that introduce the nano-cracks. Therefore, it is presumed that they are associated with the development of the nano-cracks, and it is postulated that they form by the following mechanism. The cracks cause stress relaxation in the material between them. The material below the cracks supports a tensile strain in the axial direction. Poisson's ratio effects induce a lateral contraction in the material below the cracks, which imposes a lateral compressive stress on the material between the cracks. This compressive stress, in conjunction with the modulus mismatch between the surface layer and the bulk, results in surface buckles. The mechanics of the surface buckling for this geometry is being addressed elsewhere [27].

The profiles of individual nano-cracks (or replicas of nano-cracks) were examined in detail by AFM; an example of a typical profile is shown in Fig. 14. It may be noted that the shape of the crack shown in Fig. 14 has some resemblance to the shape of cracks formed by surface diffusion [31, 32], where the rise near the crack mouth is associated with effects of surface diffusion. However, the role of diffusion in the formation of the cracks was eliminated by a series of studies where the relaxed crack profile was continually monitored by AFM for a period of eight hours after being created. Insignificantly small changes were observed in the crack geometry, leading to the conclusion that all effects discussed in this paper are dominated by elasticity. Therefore, the rise must be associated with the effects of Poisson's ratio at the crack surface. Since the crack surface relaxes in-plane strains, the out-of-plane contractions must also relax, causing the surface near the cracks to rise. The relatively smooth curves at the crack mouth were not expected for an elastic crack; these features may be associated partly with the geometry of the AFM tip. They may also be associated with the effects of surface tension deforming the relatively compliant material [33].

The cracks were characterized by three parameters: the crack spacing (the average distance to the nearest two neighbors), L; the crack opening, w; and the maximum height that the edges of the crack rise above the surface of the PDMS, r. The crack rise and opening are exterior features of the crack and could be determined with reasonable accuracy by AFM imaging of either the relaxed specimens or the replicas. The widths of the cracks are plotted as a function of the average distance to their nearest-neighbor cracks in Fig. 15a. The corresponding rises of the cracks are plotted as a function of the average distance to the nearest-neighbor cracks in Fig. 15b.

The crack depth, d, could not be determined directly since the AFM probe could not penetrate to the tip of the crack, nor was there any guarantee that the PDMS used to make

replicas of the cracked surface could flow all the way to the crack tip. Other experimental procedures were attempted in order to obtain a direct measurement of the crack depth. Sectioning (by fracture) a cracked slab of PDMS resulted in damage to the free edge of the specimen, so that attempts to image the cracked edge or a replica of the cracked edge with the AFM were unsuccessful. Bonding a cracked specimen to another oxidized piece of PDMS (in a manner similar to that discussed in Section 3.1) failed because the surface topography introduced by the cracks prevented intimate contact between the two surfaces. Finally, two slabs of oxidized PDMS were bonded together, sectioned, and then strained after bonding. This resulted in the appearance of cracks on a replica of the strained cross-section containing the bond. However, even here, it was not possible to make an accurate measurement of the crack depth. Estimates of the crack depth were eventually made by comparison to the results of finite-element calculations, as demonstrated in the following section.

4.2 Discussion

4.2.1 Effects of possible residual strain

The morphology of the nano-cracks in the relaxed specimens took two different forms. In one, the cracks were simply narrower, shorter versions of the strained cracks, with measurable widths and rises (Fig. 12). In the other, the cracks appeared to have completely but imperfectly healed, leaving the appearance of an overlapped edge (Fig. 16). The net density of the open and healed cracks on the relaxed specimens was comparable to the density of the cracks measured from the replicas taken from the corresponding strained specimens. This indicates that the origin of both types of cracks is the same—they are formed during tensile loading. The existence of open cracks after the load is removed indicates, in the absence of any obvious hysteresis effects, that there must be a residual tensile stress introduced by the oxidation process in the surface-

modified layer. The morphology of the healed relaxed cracks (Fig. 16) indicates the following further understanding of the mechanics of crack closure. While the small residual tensile stress associated with the oxidation process is often sufficient to hold open many of the cracks generated, the cracks are at a scale where they are on the border between remaining open because of the residual tension and spontaneously collapsing under the effect of surface forces. If a crack does collapse, the tension perpendicular to the crack surfaces that is associated with the surface forces induces a lateral compressive strain parallel to the crack. This local compression in conjunction with the modulus mismatch between the surface-modified layer and the substrate leads to the buckling pattern observed in Fig. 16. This understanding is supported by the observation that the period of the buckles in Fig. 16 is similar to that of the surface waves observed upon applying a tensile load to the cracked specimens.

In conclusion, the observations on the relaxed specimens indicate that the oxidation process induces a small tensile strain. This residual strain must be relatively small after a four-minute oxidation, because it is insufficient to prevent many of the cracks from collapsing. Therefore, the effects of any residual stress induced by the four minutes of oxidation are neglected in the analyses that follow. However, it was noted that specimens oxidized for a significantly longer period of time tended to form spontaneous cracks without the need to apply a tensile load. This is consistent with the notion that the increased oxidation time results in a thicker surface-modified layer or/and increased tensile strain.

4.2.2 Crack depth

In the absence of any residual strain, both the width, w, and the rise, r, of the cracks are dependent only on the properties of the system— $\overline{E}_s$, $\overline{E}_f$, and h—and on the crack spacing, L; depth, d; and applied strain, ε_{app}. Since the specimens used to produce the plots of Fig. 15 were

all oxidized at the same time, E_f and h are expected to be reasonably constant for all the data points shown. Therefore, the large variability seen for the data taken from the strained cracks at equal values of ε_{app} and L indicates a substantial variability in crack depth. It is likely that the variability in crack depth is associated with the fact that the interface between the surface-modified layer and the bulk material was not smooth (Fig. 6b).

Estimates of the crack depths were made using finite-element calculations of particular cracked geometries and the measured properties of the PDMS and surface-modified layer. An example of the appropriate model and mesh for a single crack is shown in Fig. 17. In general, the calculations should be done with asymmetrical boundary conditions, reflecting the non-uniform crack spacing. But, effects of this asymmetry were small compared with other experimental variables and were ignored. Therefore, periodic boundary conditions were used, with the lateral extent of the model being set to the average $L/2$ for the particular crack being modeled. The bulk PDMS was modeled with 2D plane-strain hybrid elements and its material behavior was modeled as hyperelastic. The experimentally determined stress/strain curve (Fig. 2) was used to define the constitutive properties. The graded surface-modified layer was modeled with 2D plane-strain linear-elastic elements; its modulus was varied from 37 MPa on the surface to 3.5 MPa at a distance of 200 nm from the surface. A displacement boundary condition was used to simulate the applied strain. The resulting width and rise of the crack were determined from the numerical output, using the same definitions as in the experiments. A series of numerical calculations were conducted with different crack depths, but keeping the crack spacing and strain corresponding to one particular set of experimental results. By comparing the numerical results for the rise and width to the experimental values, an estimate of the actual

crack depth could be obtained. This process of comparison was repeated for a number of different sets of applied strain and crack spacing.

The limited range of possible fits between the numerical results and the experimental observations indicated that the cracks had to extend beyond the thickness previously deduced for the surface-modified layer. The calculated crack depths were in the range of about 300 to 600 nm irrespective of the level of applied strain, compared to a thickness of about 200 nm for the surface-modified layer. The fact that the oxidation process may be affecting the toughness of the PDMS to depths from 150% to 300% greater than the depth to where the modulus is affected has significance for the observations of the crack spacing. If the cracks are extending well below the high-modulus region, then the crack spacing can be modeled by results for an elastically homogeneous system [28, 29]. In other words, one would expect the crack spacing to be of the order of a few multiples of the crack depth—not vastly more as would be expected for a cracked stiff layer on a compliant substrate [30]. The magnitudes of the crack spacing are not inconsistent with this conjecture.

4.2.3 *Toughness of the surface-modified layer*

The average toughness of the surface-modified layer, over a thickness corresponding to the depth of the cracks, was estimated by computing the energy-release rate of a tunneling crack. As the applied strain was increased during the tensile tests, cracks tunneled at increasing densities. A new crack can propagate between two existing cracks only if the energy-release rate for tunneling exceeds the toughness of the surface-modified layer. The stochastic nature of the distribution of the cracks and the absence of *in-situ* monitoring of the formation of the cracks results in an ambiguity in deducing the appropriate crack spacing at which to carry out analyses. Therefore, two different approaches were explored in this study. In one, the minimum average

distance to the nearest neighbors found for any crack at a given level of strain was used as the spacing at which a crack could just be propagated at that strain. In the other, this critical spacing was assumed to be given by the smallest nearest-neighbor spacing found at a given strain level. The results from both approaches were comparable.

The calculations were conducted by calculating the change in the total elastic energy between the cracked and uncracked geometry (Fig. 17). Periodic boundary conditions, suitable to each of the two different approaches, were used with applied displacements corresponding to the appropriate applied strain. The calculations were done for a range of crack depths, corresponding to those deduced earlier. The strain energy (per unit width) of the uncracked configuration was calculated, and then the strain energy (per unit width) of the cracked configuration was calculated. The energy-release rate for tunneling was found by dividing the change in energy by the crack depth. Since the energy-release rate was calculated for the extreme conditions under which cracks tunneled, this energy-release rate was directly equated to the toughness. The results of the calculations were insensitive to the particular approach used to choose the minimum crack spacing and produced an estimate of the toughness in the range of 100 to 300 mJ/m^2. This remarkably low toughness—a drop by three orders of magnitude from the bulk value for the PDMS of about 250–300 J/m^2—indicates a significant embrittling of the surface layer by the oxidation. Chaudhury and Whitesides [34] estimated the free surface energy, γ_s, of plasma-oxidized PDMS to be approximately 60 mJ/m^2. Therefore, the calculated toughness range is very close to $2\gamma_s$, which indicates that the surface-modified layer is almost perfectly brittle. This is in contrast to the relatively high toughness of the bulk PDMS, which indicates some crack-tip dissipative mechanisms, probably pull out of the molecular chains.

5 Concluding remarks

A relatively quick and simple method has been demonstrated for determining the thickness and elastic modulus of the surface-modified layer created on PDMS by exposure to plasma oxygen. This method takes advantage of a substantial modulus mismatch between the stiff surface-modified layer and the compliant substrate to interpret the results of two different AFM probing techniques. The first uses the phase shift in the tapping-mode cantilever vibration when passing over the two different regions on the cross-section of oxidized PDMS to measure the thickness of the surface-modified layer. The second utilizes the solution of plate bending on an elastic foundation under a point load exerted by the AFM probe to deduce the elastic modulus of the surface-modified layer. Using these methods, a surface-modified layer created by four minutes of exposure to oxygen plasma was determined to have a modulus varying from about 37 MPa at the surface to a bulk value of 3.5 MPa at a depth of about 200 nm below the surface.

An array of parallel nano-cracks is produced within the surface-modified layer upon the application of a uniaxial tensile strain. The crack spacing decreased with increased applied uniaxial tensile strain as expected from existing analyses of cracking in thin films. While the depth of the cracks could not be determined directly, it could be estimated by comparing experimental observations of the crack opening, surface rise, and spacing with finite-element calculations for these quantities using the measured properties of the surface layer. These estimates indicated that there was a stochastic variation in the crack depth, without any systematic effect of applied strain. The surface layer was essentially perfectly brittle with a calculated toughness of about 100–300 mJ/m^2 to a depth of about 300–600 nm below the surface. The lower bound of this toughness is about twice the reported free surface energy of oxidized PDMS. Finally, it was noted that the oxidation process produced a very small level of residual

tensile stress; however, this was too small to prevent the majority of the cracks from collapsing upon unloading.

Acknowledgements

We thank the NIH (EB003793-01) for funding and Dr. J. R. Barber and Donghee Lee for valuable discussion.

References

1. Lotters, J.C., W. Olthuis, P.H. Veltink, and P. Bergveld: The mechanical properties of the rubber elastic polymer polydimethylsiloxane for sensor applications. *J. Micromech. Microeng.* **7**, 145 (1997).

2. Bietsch, A. and B. Michel: Conformal contact and pattern stability of stamps used for soft lithography. *J. Appl. Phys.* **88**, 4310 (2000).

3. Kumar, A., H.A. Biebuyck, and G.M. Whitesides: Patterning self-assembled monolayers: Applications in materials science. *Langmuir* **10**, 1498 (1994).

4. Duffy, D.C., J.C. McDonald, O.J.A. Schueller, and G.M. Whitesides: Rapid prototyping of microfluidic systems in poly(dimethlysiloxane). *Anal. Chem.* **70**, 4974 (1998).

5. Gu, W., X.Y. Zhu, N. Futai, B.S. Cho, and S. Takayama: Computerized microfluidic cell culture using elastomeric channels and Braille displays. *Proc. Natl. Acad. Sci. U. S. A.* **101**, 15861 (2004).

6. Unger, M.A., H.-P. Chou, T. Thorsen, A. Scherer, and S.R. Quake: Monolithic microfabricated valves and pumps by multilayer soft lithography. *Science* **288**, 113 (2000).

7. Fritz, J.L. and M.J. Owen: Hydrophobic recovery of plasma-treated polydimethylsiloxane. *J. Adhes.* **54**, 33 (1995).

8. Hillborg, H. and U.W. Gedde: Hydrophobicity changes in silicone rubbers. *IEEE Trns. Dielectr. Electr. Insul.* **6**, 703 (1999).

9. Bowden, N., W.T.S. Huck, K.E. Paul, and G.M. Whitesides: The controlled formation of ordered, sinusoidal structures by plasma oxidation of an elastomeric polymer. *Appl. Phys. Lett.* **75**, 2557 (1999).

10. Efimenko, K., M. Rackaitis, E. Manias, A. Vaziri, L. Mahadevan, and J. Genzer: Nested self-similar wrinkling patterns in skins. *Nat. Mater.* **4**, 293 (2005).

11. Hillborg, H., J.F. Ankner, U.W. Gedde, G.D. Smith, H.K. Yasuda, and K. Wikstrom: Crosslinked polydimethylsiloxane exposed to oxygen plasma studied by neutron reflectometry and other surface specific techniques. *Polymer* **41**, 6851 (2000).

12. Zhu, X.Y., K.L. Mills, P.R. Peters, J.H. Bahng, E.H. Liu, J. Shim, K. Naruse, M.E. Csete, M.D. Thouless, and S. Takayama: Fabrication of reconfigurable protein matrices by cracking. *Nature Materials* **4**, 403 (2005).

13. Huh, D., K.L. Mills, X. Zhu, M.A. Burns, M.D. Thouless, and S. Takayama: Reconfigurable elastomeric nanochannels for tunable nanofluidic manipulation. *Manuscript submitted for publication*, (2007).

14. Hillborg, H., N. Tomczak, A. Olah, H. Schonherr, and G.J. Vancso: Nanoscale hydrophobic recovery: A chemical force microscopy study of UV/ozone-treated cross-linked poly(dimethylsiloxane). *Langmuir* **20**, 785 (2004).

15. Bhattacharya, A.K. and W.D. Nix: Analysis of elastic and plastic-deformation associated with indentation testing of thin-films on substrates. *Int. J. Solids Struct.* **24**, 1287 (1988).

16. Saha, R. and W.D. Nix: Effects of the substrate on the determination of thin film mechanical properties by nanoindentation. *Acta Mater.* **50**, 23 (2002).

17. Whitesides, G.M., E. Ostuni, S. Takayama, X.Y. Jiang, and D.E. Ingber: Soft lithography in biology and biochemistry. *Annu. Rev. Biomed. Eng.* **3**, 335 (2001).

18. Bar, G., L. Delineau, A. Hafele, and M.-H. Whangbo: Investigation of the stiffness change in, the indentation force and the hydrophobic recovery of plama-oxidized polydimethylsiloxane surfaces by tapping mode atomic force microscopy. *Polymer* **42**, 3627 (2001).

19. Babcock, K.L. and C.B. Prater: Phase imaging: beyond topography. *MultiMode AFM Application Notes*, (Veeco Instruments, Inc., Santa Barbara, CA, 2004).

20. Clement, F., A. Lapra, L. Bokobza, L. Monnerie, and P. Menez: Atomic force microscopy investigation of filled elastomers and comparison with transmission electron microscopy - application to silica-filled silicone elastomers. *Polymer* **42**, 6259 (2001).

21. Magonov, S.N., V. Elings, and M.-H. Whangbo: Phase imaging and stiffness in tapping-mode atomic force microscopy. *Surf. Sci.* **375**, L385 (1997).

22. Mills, K.L., X. Zhu, D. Lee, S. Takayama, and M.D. Thouless: Properties of the surface-modified layer of plasma-oxidized poly(dimethylsiloxane), in *Mechanics of Nanoscale Materials and Devices*, edited by A. Misra, J.P. Sullivan, H. Huang, K. Lu, and S. Asif. (Mater. Res. Soc. Symp. Proc. **924E**, San Francisco, CA, 2006).

23. Oliver, W.C. and G.M. Pharr: An improved technique for determining hardness and elastic-modulus using load and displacement sensing indentation experiments. *J. Mater. Res.* **7**, 1564 (1992).

24. Olshanskii, V.P.: Green's function for the bending of a plate on an elastic half-space. *Pmm-J. Appl. Math. Mech.* **51**, 681 (1987).

25. Allen, H.G.: *Analysis and design of structural sandwich panels*. 1st ed., (Pergamon Press, Oxford, 1969).

26. Huang, Z.Y., W. Hong, and Z. Suo: Nonlinear analyses of wrinkles in a film bonded to a compliant substrate. *J. Mech. Phys. Solids* **53**, 2101 (2005).

27. Lee, D., N. Triantafyllidis, J.R. Barber, and M.D. Thouless: *Unpublished work*, (2007).

28. Thouless, M.D., E. Olsson, and A. Gupta: Cracking of Brittle Films on Elastic Substrates. *Acta Metall. Mater.* **40**, 1287 (1992).

29. Thouless, M.D.: Crack spacing in brittle films on elastic substrates. *J. Am. Ceram. Soc.* **73**, 2144 (1990).

30. Shenoy, V.B., A.F. Schwartzman, and L.B. Freund: Crack patterns in brittle thin films. *Int. J. Fract.* **103**, 1 (2000).

31. Mullins, W.W.: Theory of thermal grooving. *J. Appl. Phys.* **28**, 333 (1957).

32. Thouless, M.D.: Effect of surface-diffusion on the creep of thin-films and sintered arrays of particles. *Acta Metall. Mater.* **41**, 1057 (1993).

33. Hui, C.Y., A. Jagota, Y.Y. Lin, and E.J. Kramer: Constraints on microcontact printing imposed by stamp deformation. *Langmuir* **18**, 1394 (2002).

34. Chaudhury, M.K. and G.M. Whitesides: Direct measurement of interfacial interactions between semispherical lenses and flat sheets of poly(dimethylsiloxane) and their chemical derivatives. *Langmuir* **7**, 1013 (1991).

Figure Captions

Figure 1 Tensile specimen for the determination of the constitutive properties of the bulk PDMS material. The thickness of the PDMS sheets was 2.0 ± 0.2 mm. The gage length of 18.5 mm was drawn directly onto each specimen.

Figure 2 Range of nominal stress versus strain curves obtained from the tensile experiments performed on the bulk PDMS. The strain rate of the samples for the curves shown here was approximately $0.02\ s^{-1}$; although, it was determined that the PDMS constitutive behavior demonstrated a negligible dependence on strain rate. The average of the failure strains for the unoxidized (○) and oxidized (●) samples were 80% and 68%, respectively.

Figure 3 (a) Trouser test specimen geometry for measuring the mode-III fracture toughness of the bulk PDMS. Indicated on the figure are the initial leg length (pre-crack) of 40 mm and the path along which a score was placed (dashed line) to ensure that the fracture remained in tearing mode. The tearing load, F_t, was independent of the overall length of the specimens which varied between 90 and 125 mm. (b) The arrangement of trouser specimen during loading.

Figure 4 Compact-tension specimen geometry for measuring the mode-I fracture toughness of the bulk PDMS as specified in ASTM Standard D5045–99. The specimen is loaded at the pin connectors so that the crack mouth is pulled open while measuring the accompanying load.

Figure 5 Loading curves from the compact tension tests. A constant displacement rate of 1 mm/s was applied at the pin points to open the crack mouth.

Figure 6 AFM (a) phase and (b) height images of the same region of the cross-section containing the bond between the surface of PDMS oxidized for one minute (on the left) and the surface oxidized for four minutes (on the right). (c) Line trace of the phase angle across the bond at the location of the marker on the phase image in Figure 6a. The thickness of the surface-modified layer was measured from the lowest point of the phase angle, at the bond line, to the average value for the bulk material.

Figure 7 Load versus indentation depth curve for the stiff cantilever ($k = 40$ N/m) indenting on the surface-modified layer of PDMS. The indentation depth was greater than ten times the measured thickness of the surface-modified layer and the shape of the curve is reminiscent of a characteristic plastic indent.

Figure 8 The load versus indentation relationship for the compliant cantilever ($k = 0.58$ N/m) indenting on unoxidized PDMS showed typical contact mechanics of elastic indentation with no apparent hysteresis between the indentation and retraction portions of the curve. Subsequent imaging did not reveal any permanent damage on the unmodified surface of the PDMS.

Figure 9 The load versus indentation depth relationship for the compliant cantilever ($k = 0.58$ N/m) indenting on oxidized PDMS is linear as shown by this example of the relationship between cantilever deflection and z-piezo travel distance. The indentation curve is the solid and the retraction curve is the dashed line.

Figure 10 The range of load versus indentation depth curves for all indents taken in various positions on the surface-modified layer of one PDMS sample that had been oxidized for four minutes.

Figure 11 Average crack spacing versus applied strain. Data taken from molds made of strained specimens are indicated by solid circles (●). Data taken from direct measurements of relaxed specimens are indicated by open circles (○).

Figure 12 AFM image of the relaxed nano-cracks introduced into the surface-modified layer of PDMS by the application of a 10% applied tensile strain.

Figure 13 AFM image of the PDMS mold of strained nano-cracks with the accompanying surface buckling. These nano-cracks were created by the application of 15% applied tensile strain in the direction perpendicular to the cracks.

Figure 14 A typical profile of a nano-crack obtained with the AFM. This particular profile has been vertically reversed from the data taken from a mold of a specimen strained to 10%. The width, w, and rise, r, of the cracks were measured as indicated.

Figure 15 (a) Crack widths, w, and (b) crack rises, r, were experimentally measured when possible from the molds of strained specimen and are plotted against the average nearest neighbor crack spacing, L, for 6% (∇), 10% (○),15% (□), 20% (◊), and 30% (Δ) applied strain.

Figure 16 These healed relaxed cracks are on the surface of a relaxed specimen which had been strained to 20%. The cracks collapse due to surface forces acting on the crack faces. Tension induced at the edges of the cracks causes the appearance of buckling. The wavelength of the buckled edge is consistent with the buckling wavelength on the molds of the strained cracks.

Figure 17 Finite-element mesh used for fitting the width and rise of the cracks to both find the depth of penetration of the cracks and to estimate the average toughness of the surface-modified layer. The lateral dimension on either side of the crack is L/2 for the appropriate crack spacing being modeled. The crack depth can be fixed to anywhere in the region marked d_o. Using the average spacing approach, only half of the crack is modeled and the appropriate periodic boundary condition is applied at the plane corresponding to the crack face.

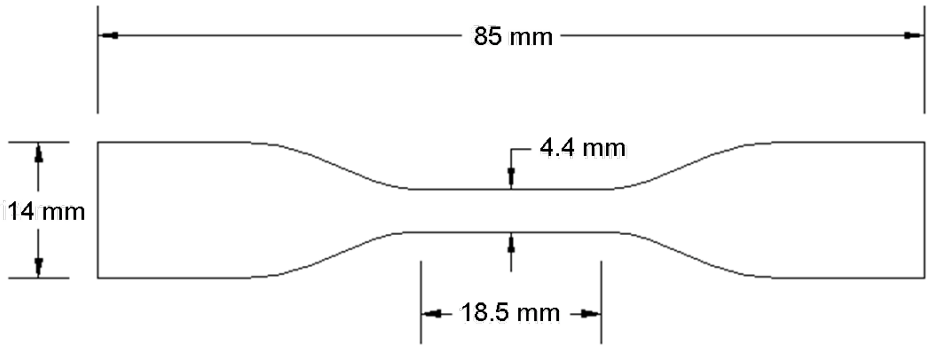

Figure 1 Tensile specimen for the determination of the constitutive properties of the bulk PDMS material. The thickness of the PDMS sheets was 2.0 ± 0.2 mm. The gage length of 18.5 mm was drawn directly onto each specimen.

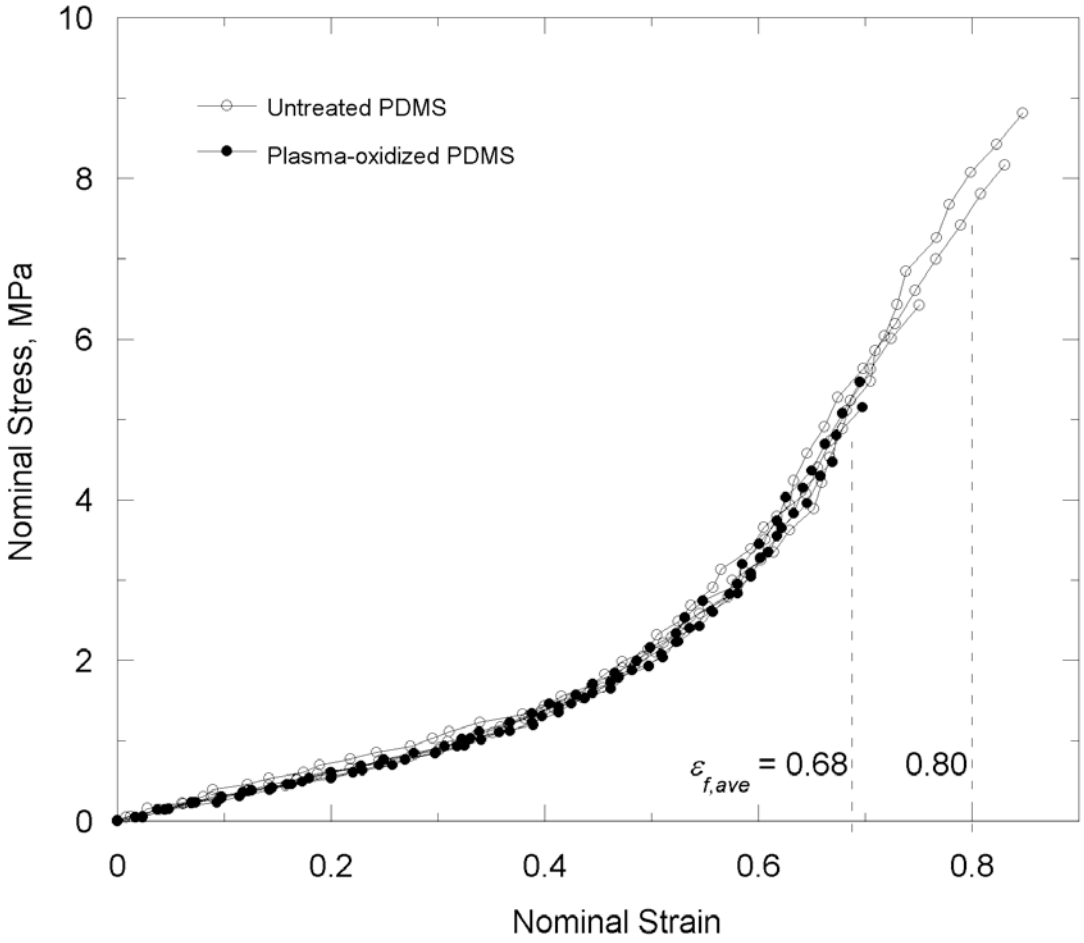

Figure 2 Range of nominal stress versus strain curves obtained from the tensile experiments performed on the bulk PDMS. The strain rate of the samples for the curves shown here was approximately 0.02 s^{-1}; although, it was determined that the PDMS constitutive behavior demonstrated a negligible dependence on strain rate. The average of the failure strains for the unoxidized (○) and oxidized (●) samples were 80% and 68%, respectively.

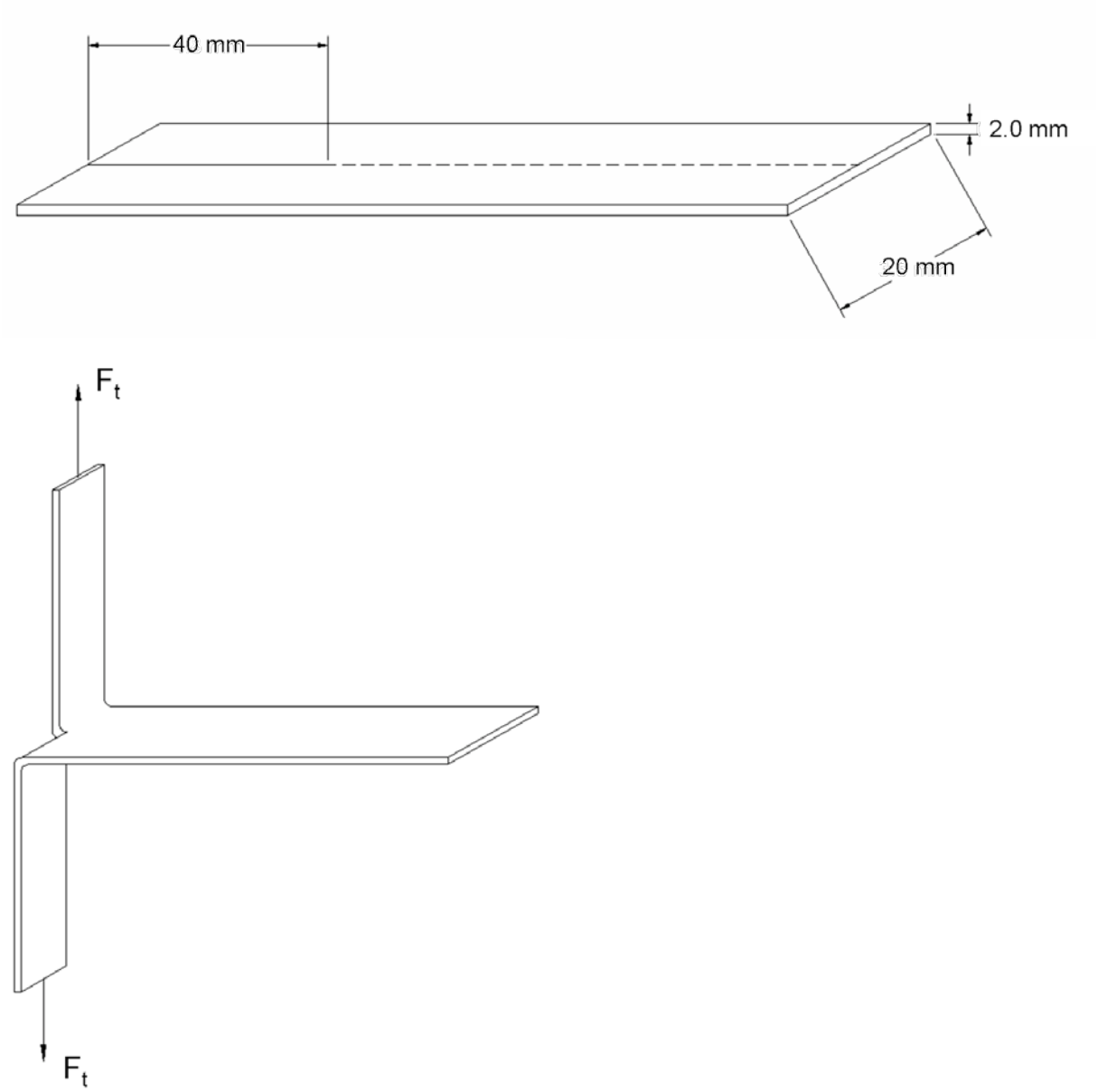

Figure 3 (a) Trouser test specimen geometry for measuring the mode-III fracture toughness of the bulk PDMS. Indicated on the figure are the initial leg length (pre-crack) of 40 mm and the path along which a score was placed (dashed line) to ensure that the fracture remained in tearing mode. The tearing load, F_t, was independent of the overall length of the specimens which varied between 90 and 125 mm. (b) The arrangement of trouser specimen during loading.

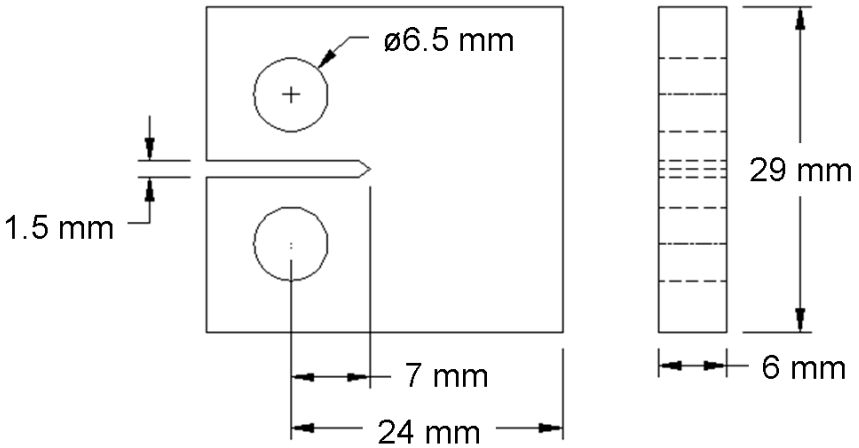

Figure 4 Compact-tension specimen geometry for measuring the mode-I fracture toughness of the bulk PDMS as specified in ASTM Standard D5045 - 99. The specimen is loaded at the pin connectors so that the crack mouth is pulled open while measuring the accompanying load.

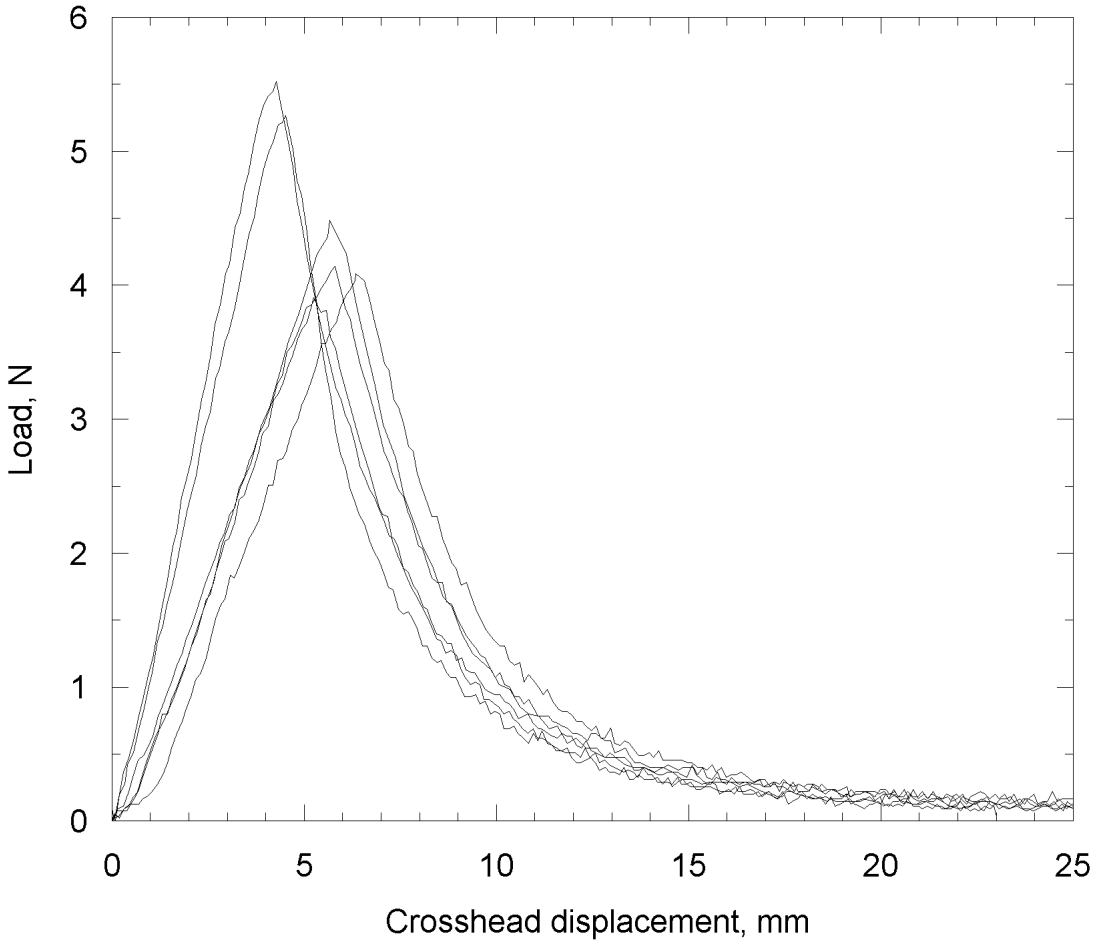

Figure 5 Loading curves from the compact tension tests. A constant displacement rate of 1 mm/s was applied at the pin points to open the crack mouth.

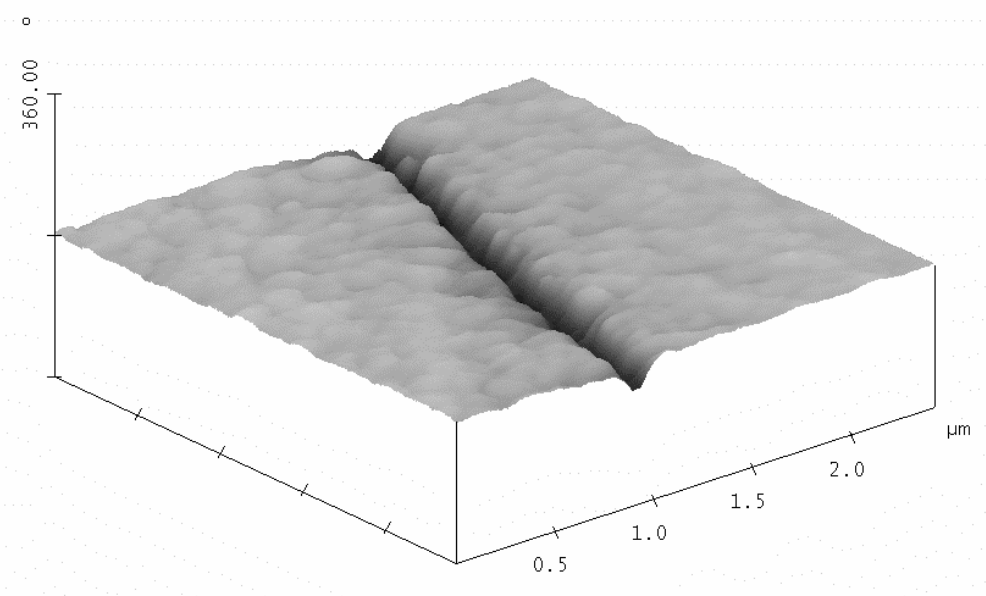

Figure 6a (3d) OR…

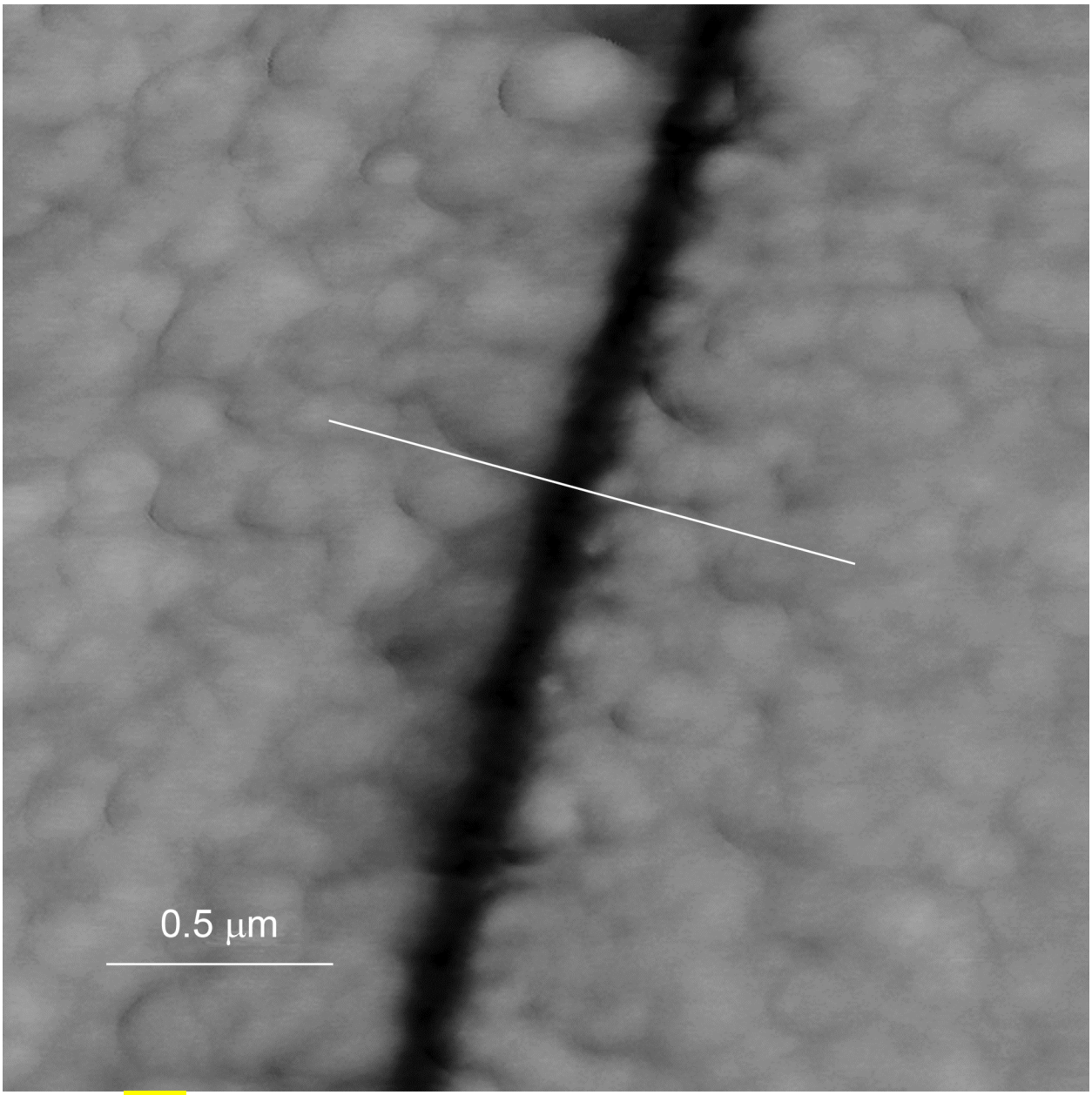

Figure 6a (2d)?

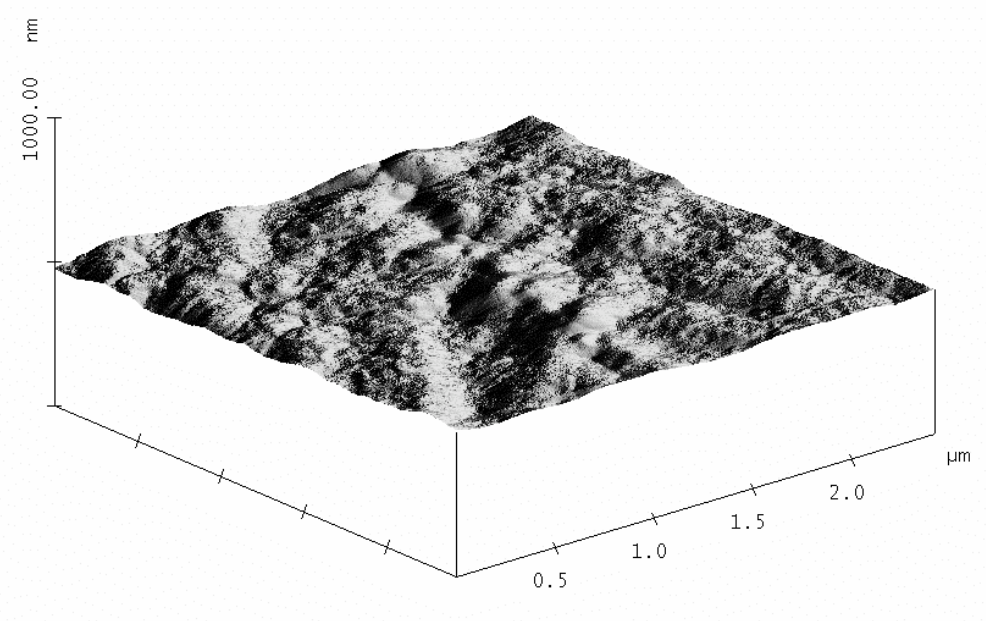

Figure 6b (3d) OR…

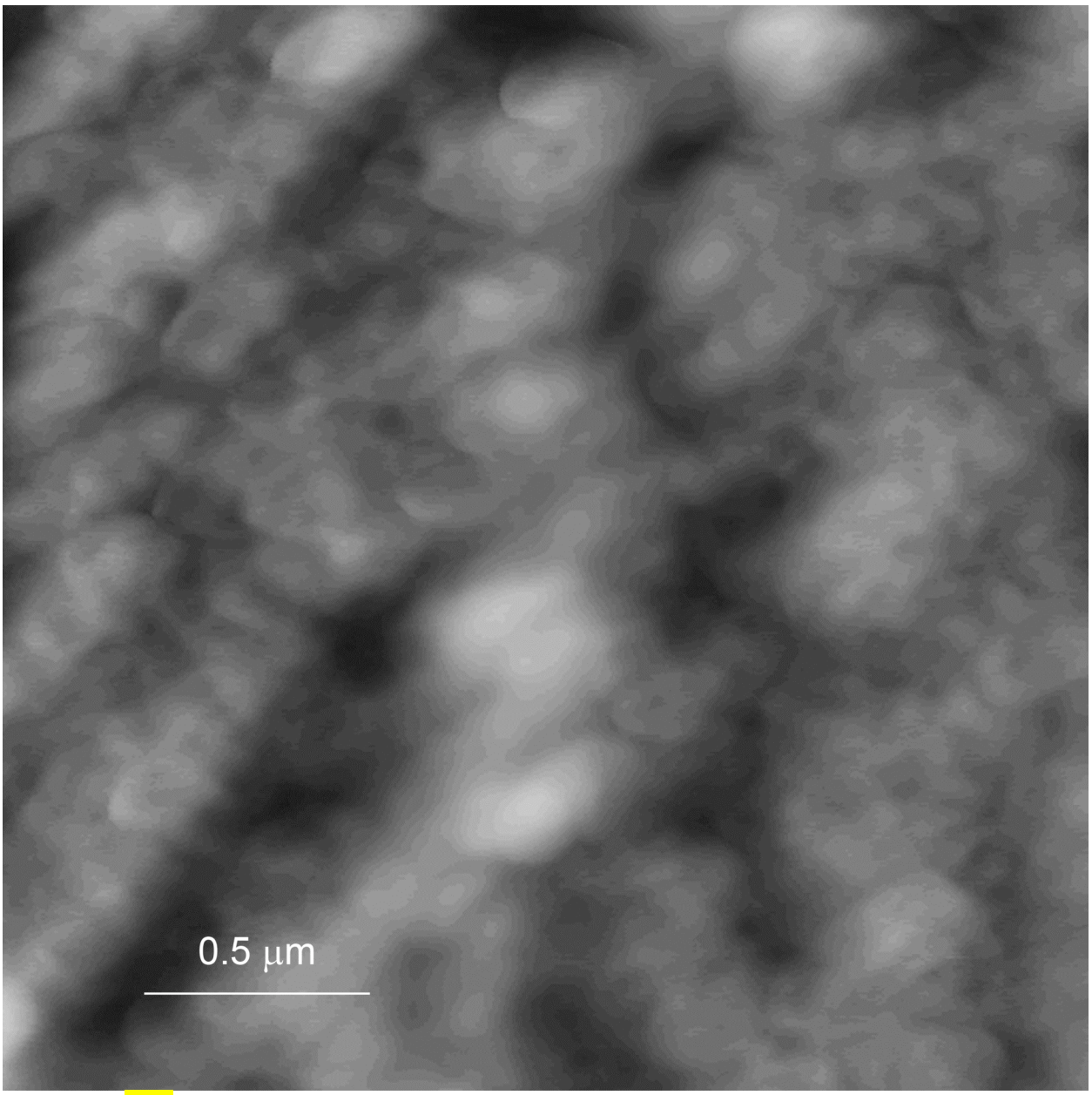

Figure 6b (2d)

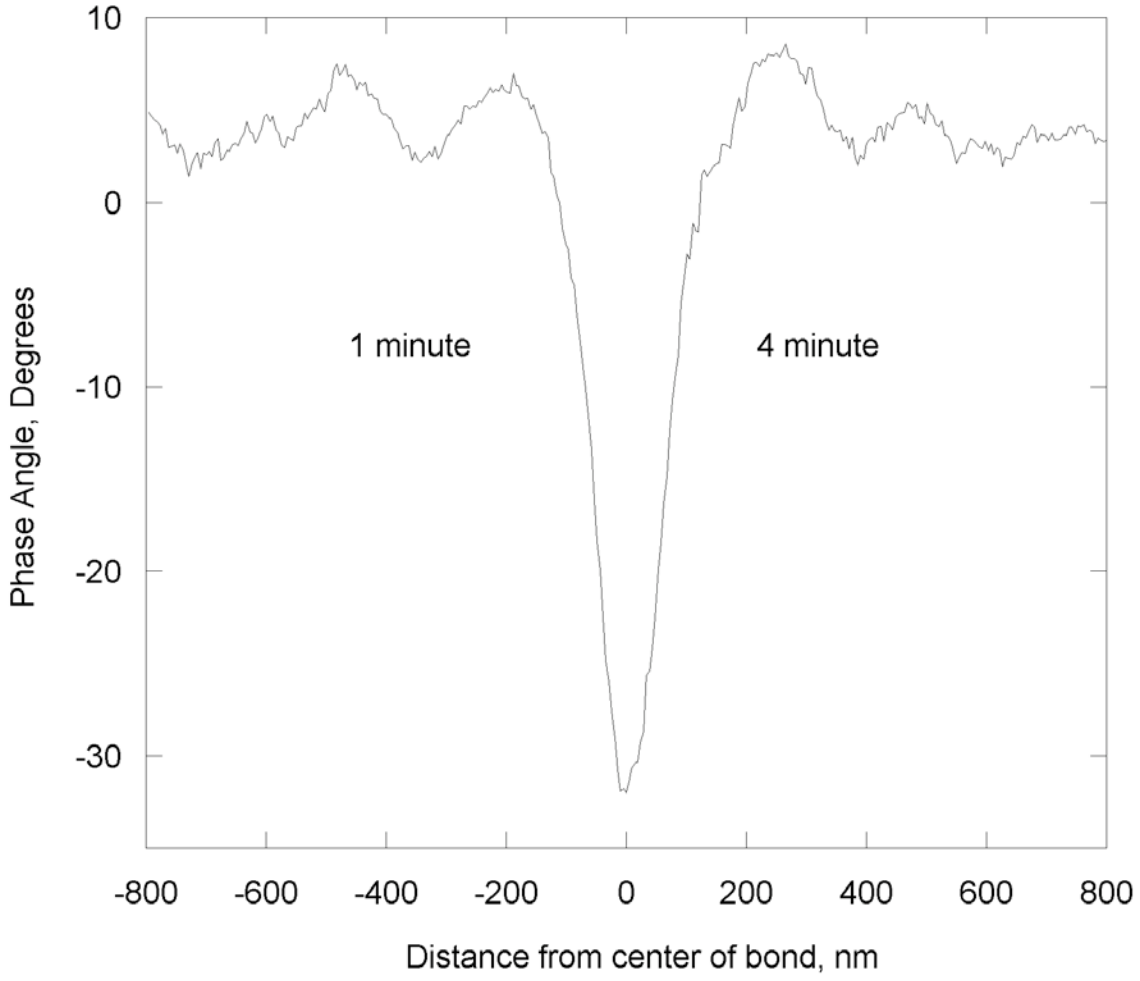

Figure 6c

Figure 6 AFM (a) phase and (b) height images of the same region of the cross-section containing the bond between the surface of PDMS oxidized for one minute (on the left) and the surface oxidized for four minutes (on the right). (c) Line trace of the phase angle across the bond at the location of the marker on the phase image in Figure 6a. The thickness of the surface-modified layer was measured from the lowest point of the phase angle, at the bond line, to the average value for the bulk material.

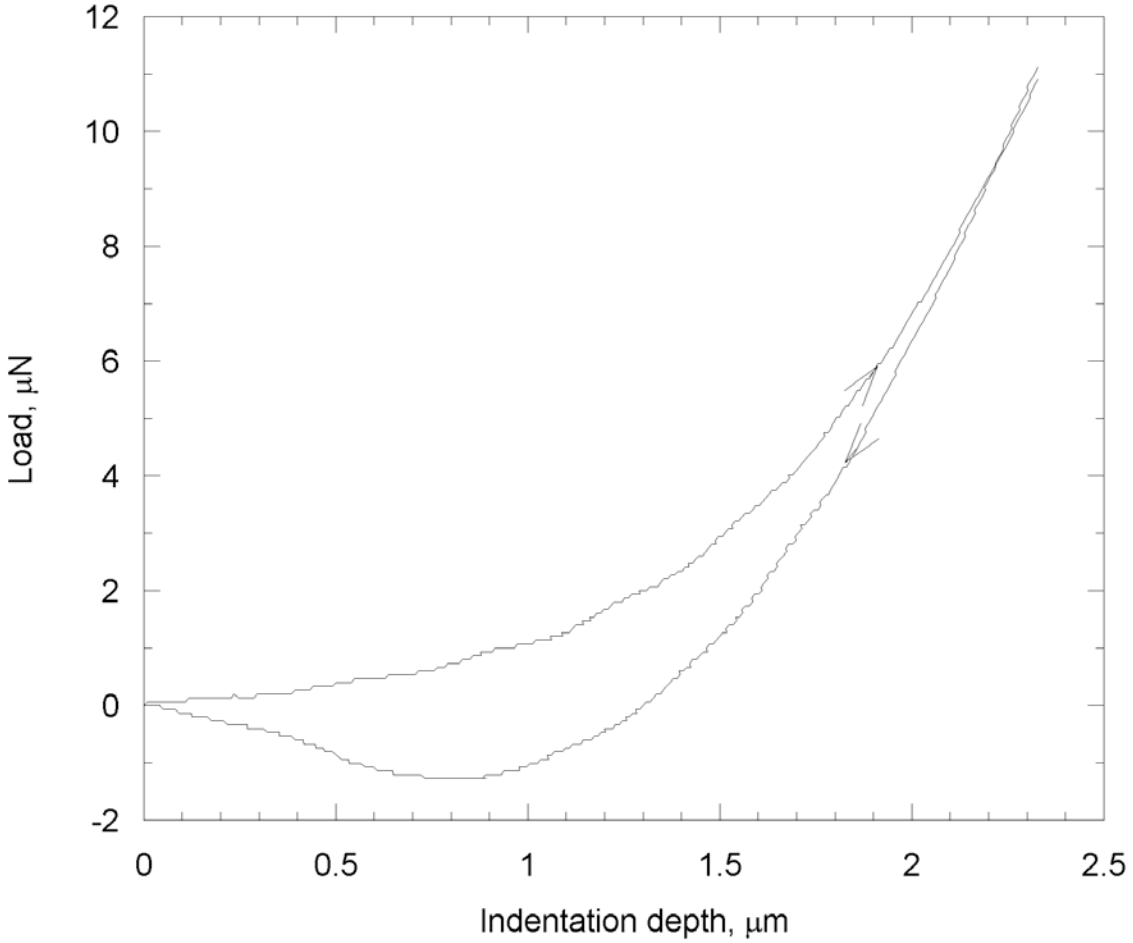

Figure 7 Load versus indentation depth curve for the stiff cantilever (k = 40 N/m) indenting on the surface-modified layer of PDMS. The indentation depth was greater than ten times the measured thickness of the surface-modified layer and the shape of the curve is reminiscent of a characteristic plastic indent.

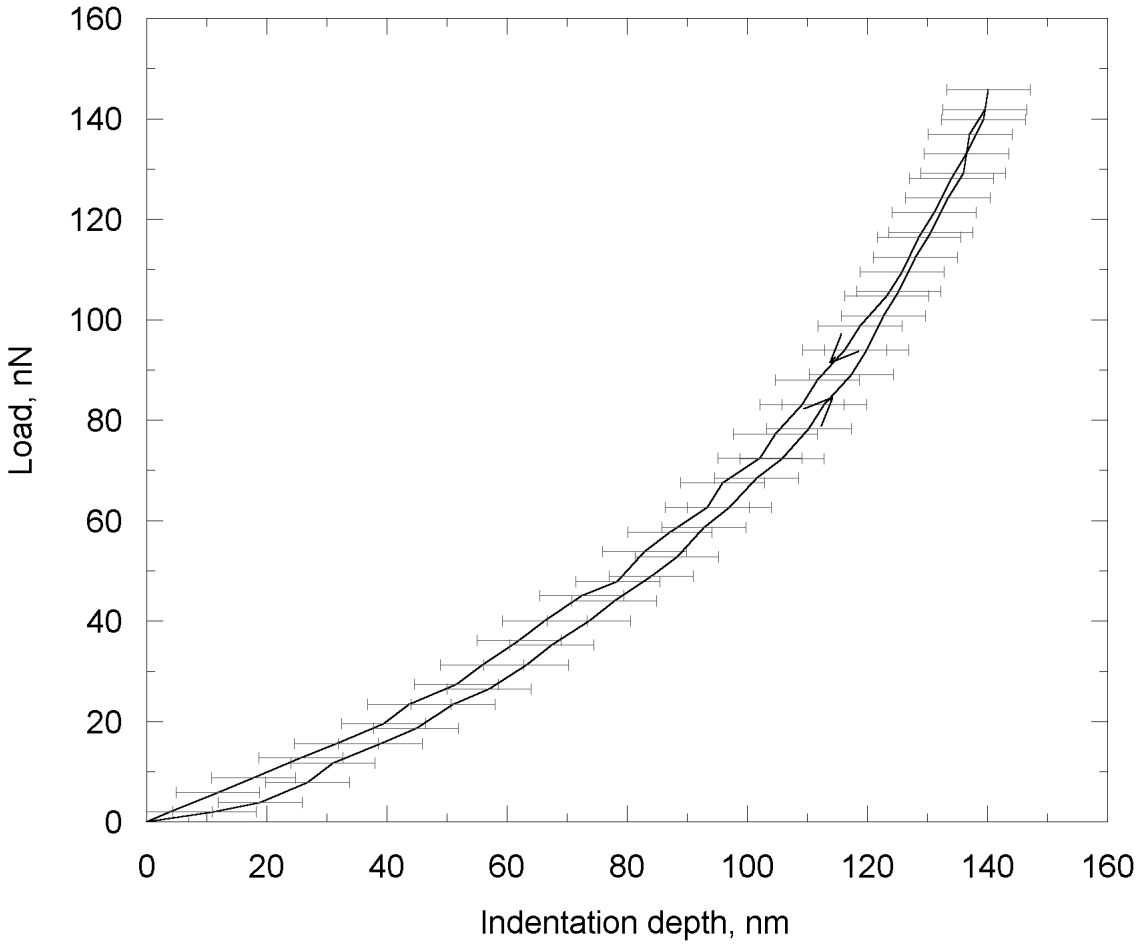

Figure 8 The load versus indentation relationship for the compliant cantilever (k = 0.58 N/m) indenting on unoxidized PDMS showed typical contact mechanics of elastic indentation with no apparent hysteresis between the indentation and retraction portions of the curve. Subsequent imaging did not reveal any permanent damage on the unmodified surface of the PDMS.

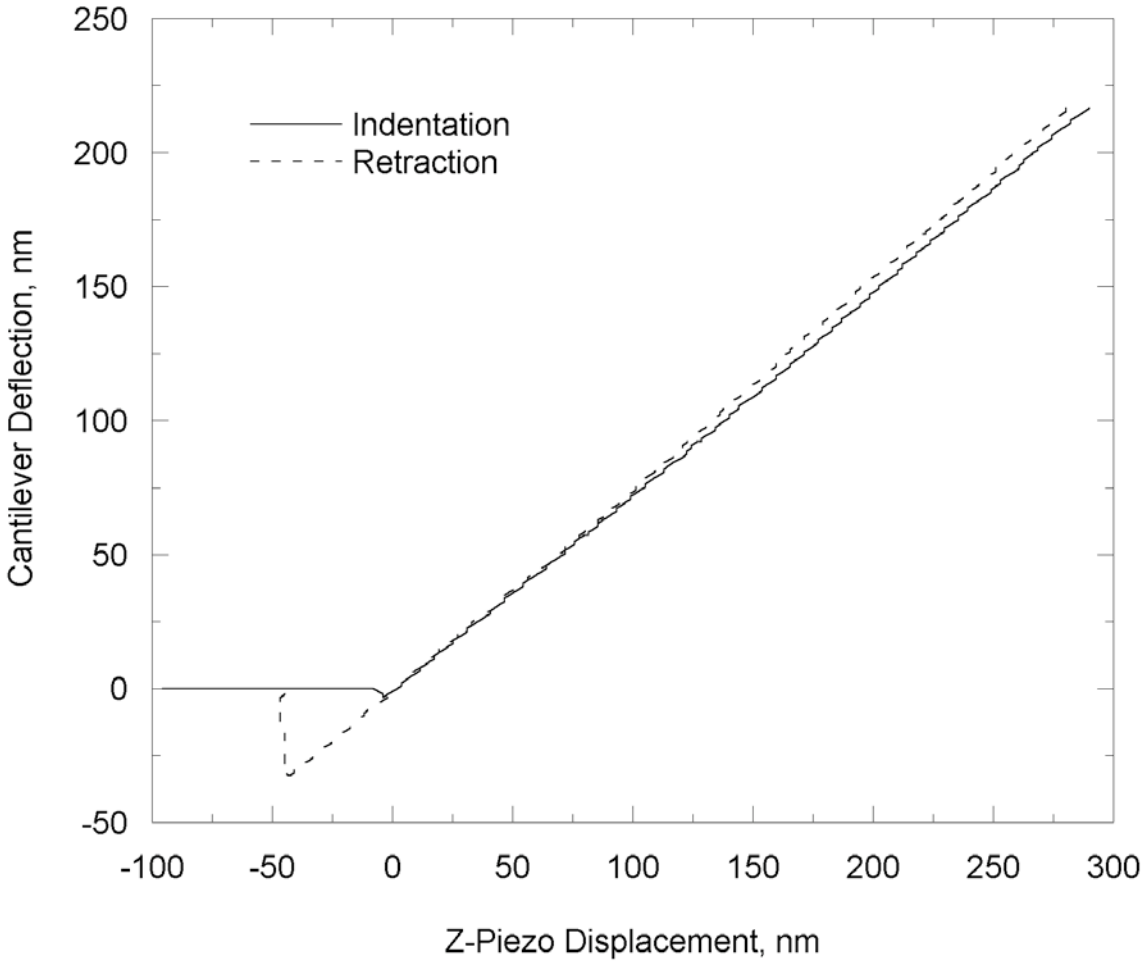

Figure 9 The load versus indentation depth relationship for the compliant cantilever (k = 0.58 N/m) indenting on oxidized PDMS is linear as shown by this example of the relationship between cantilever deflection and z-piezo travel distance. The indentation curve is the solid and the retraction curve is the dashed line.

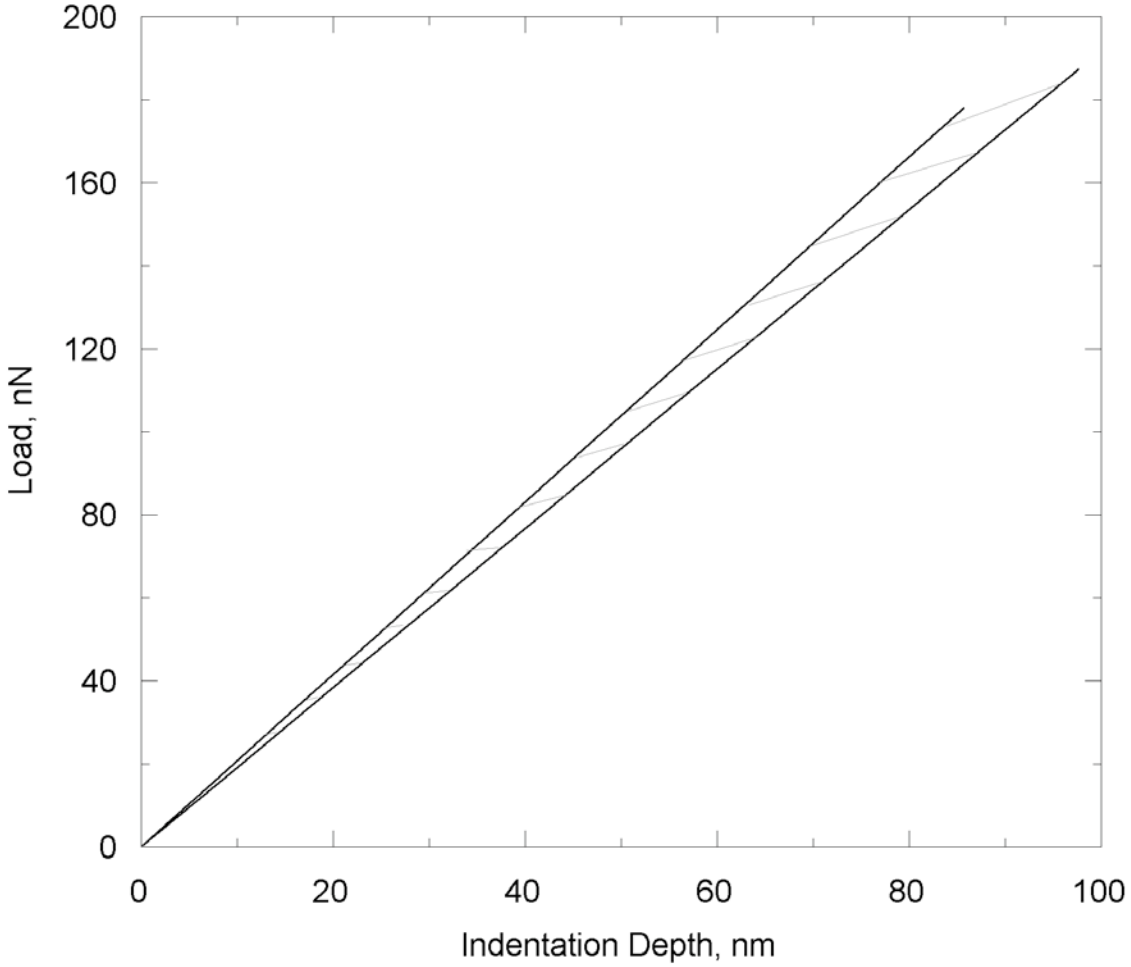

Figure 10 The range of load versus indentation depth curves for all indents taken in various positions on the surface-modified layer of one PDMS sample that had been oxidized for four minutes.

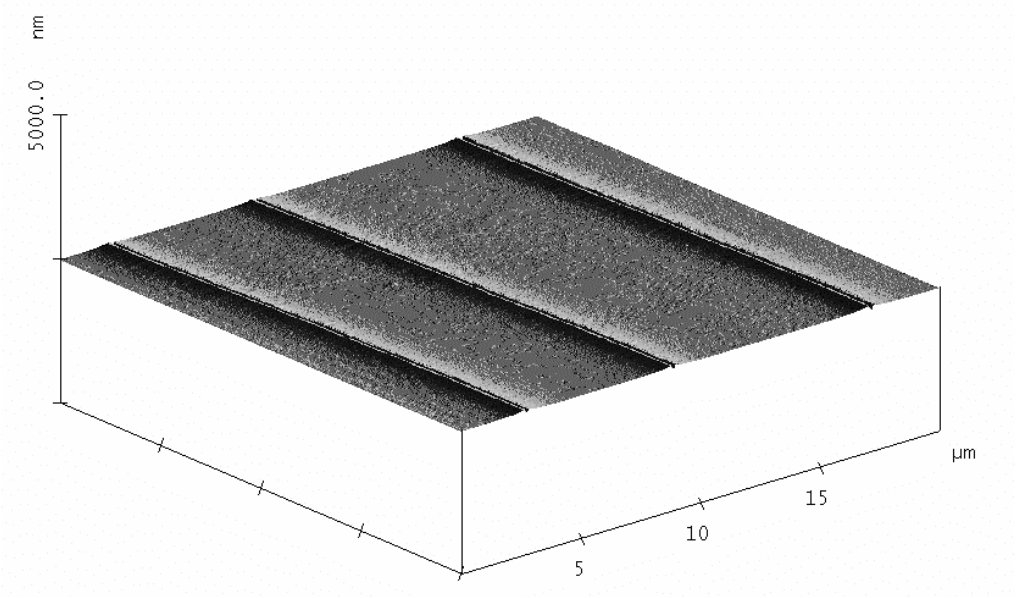

Figure 11 AFM image of the relaxed nano-cracks introduced into the surface-modified layer of PDMS by the application of a 10% applied tensile strain.

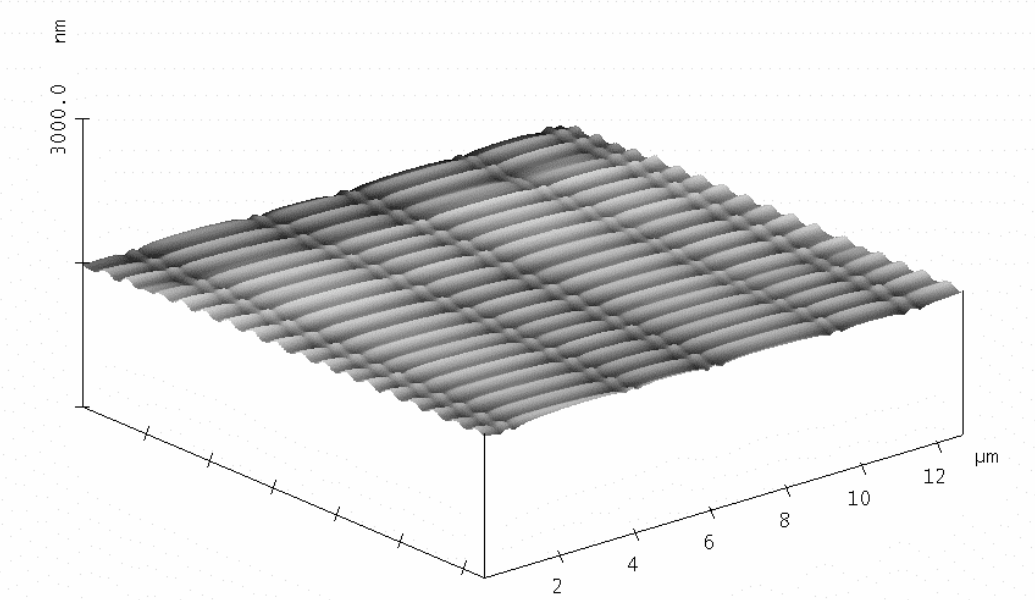

Figure 12 AFM image of the PDMS mold of strained nano-cracks with the accompanying surface buckling. These nano-cracks were created by the application of 15% applied tensile strain in the direction perpendicular to the cracks.

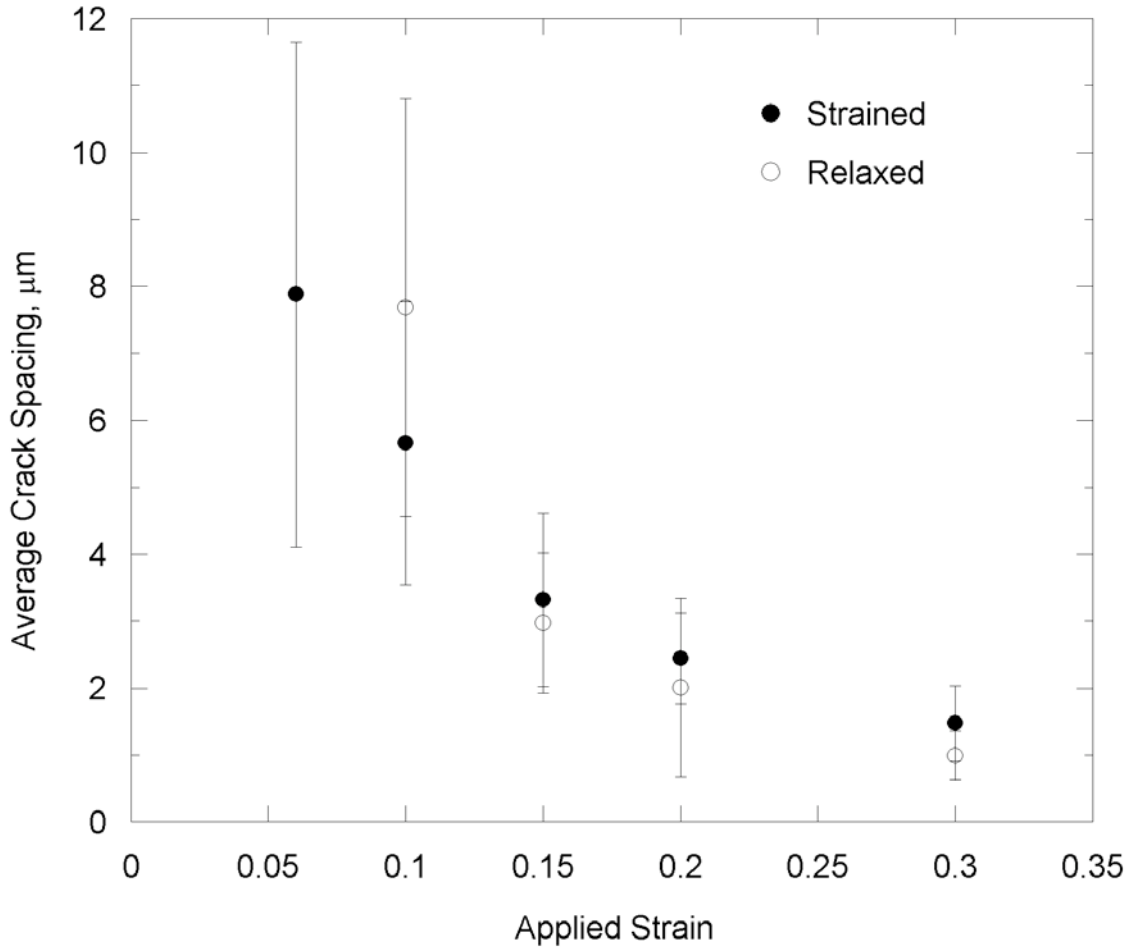

Figure 13 Average crack spacing versus applied strain. Data taken from molds made of strained specimens are indicated by solid circles (●). Data taken from direct measurements of relaxed specimens are indicated by open circles (○).

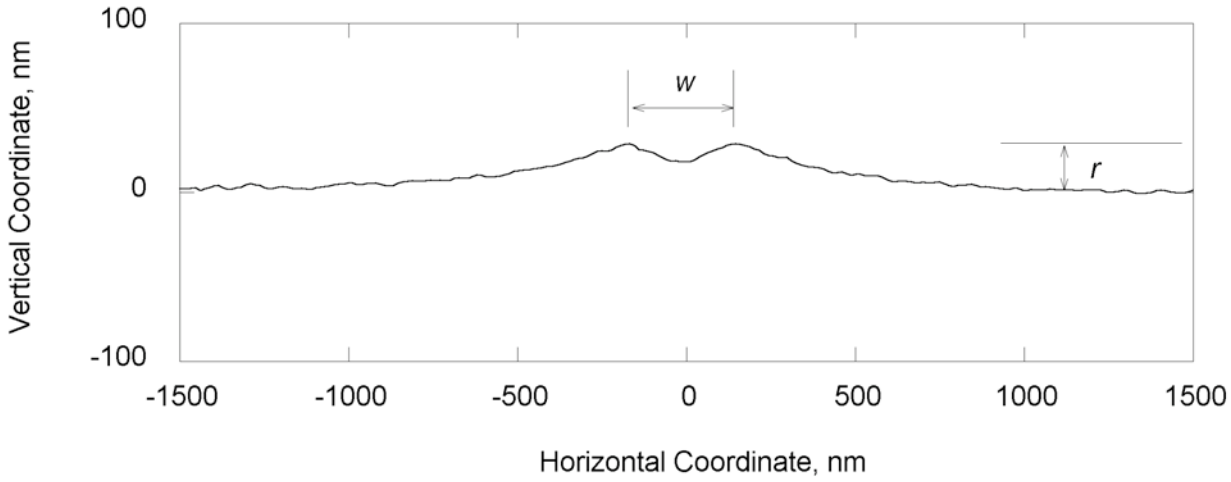

Figure 14 A typical profile of a nano-crack obtained with the AFM. This particular profile has been vertically reversed from the data taken from a mold of a specimen strained to 10%. The width, *w*, and rise, *r*, of the cracks were measured as indicated.

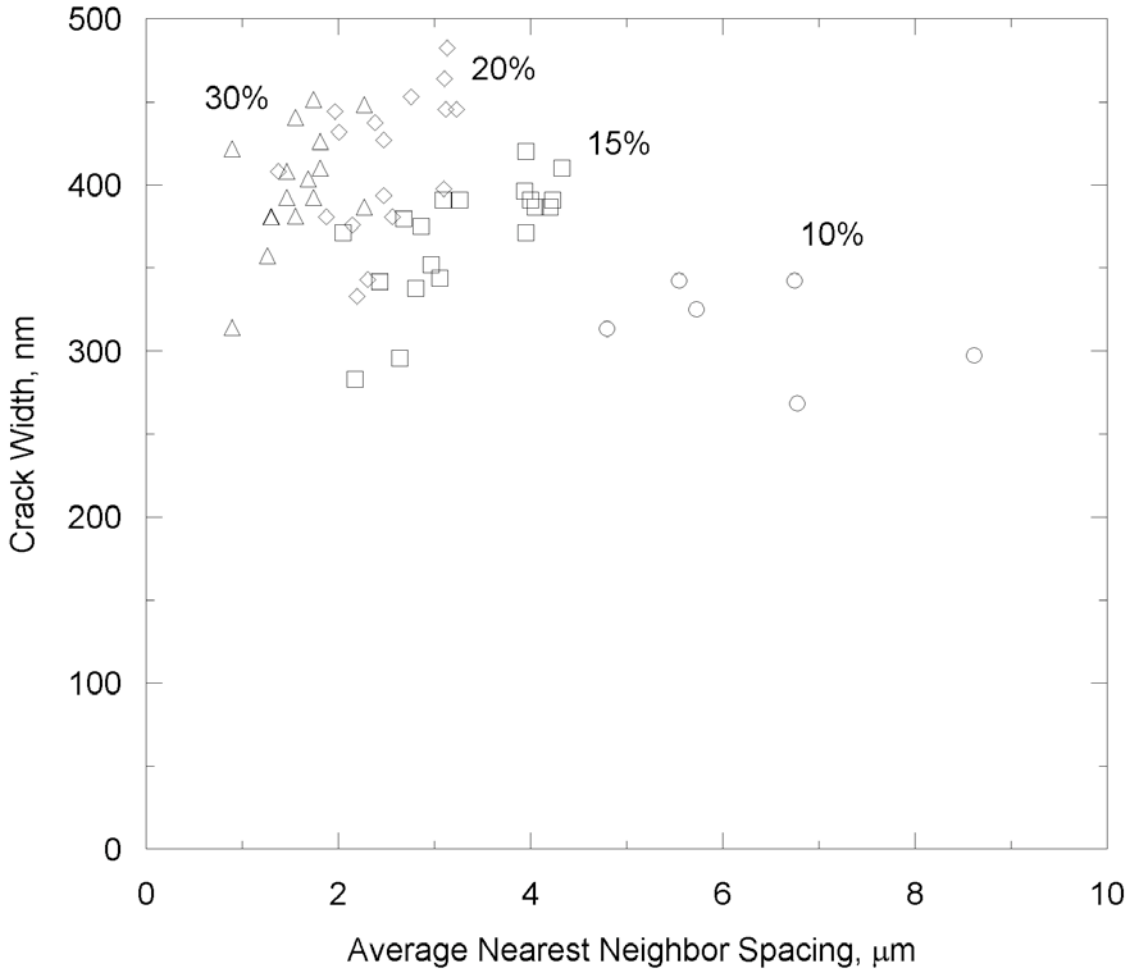
500
400
300
200
100
0
Crack Width, nm
0
2
4
6
8
10
Average Nearest Neighbor Spacing, μm
30%
20%
15%
10%

Figure 15a

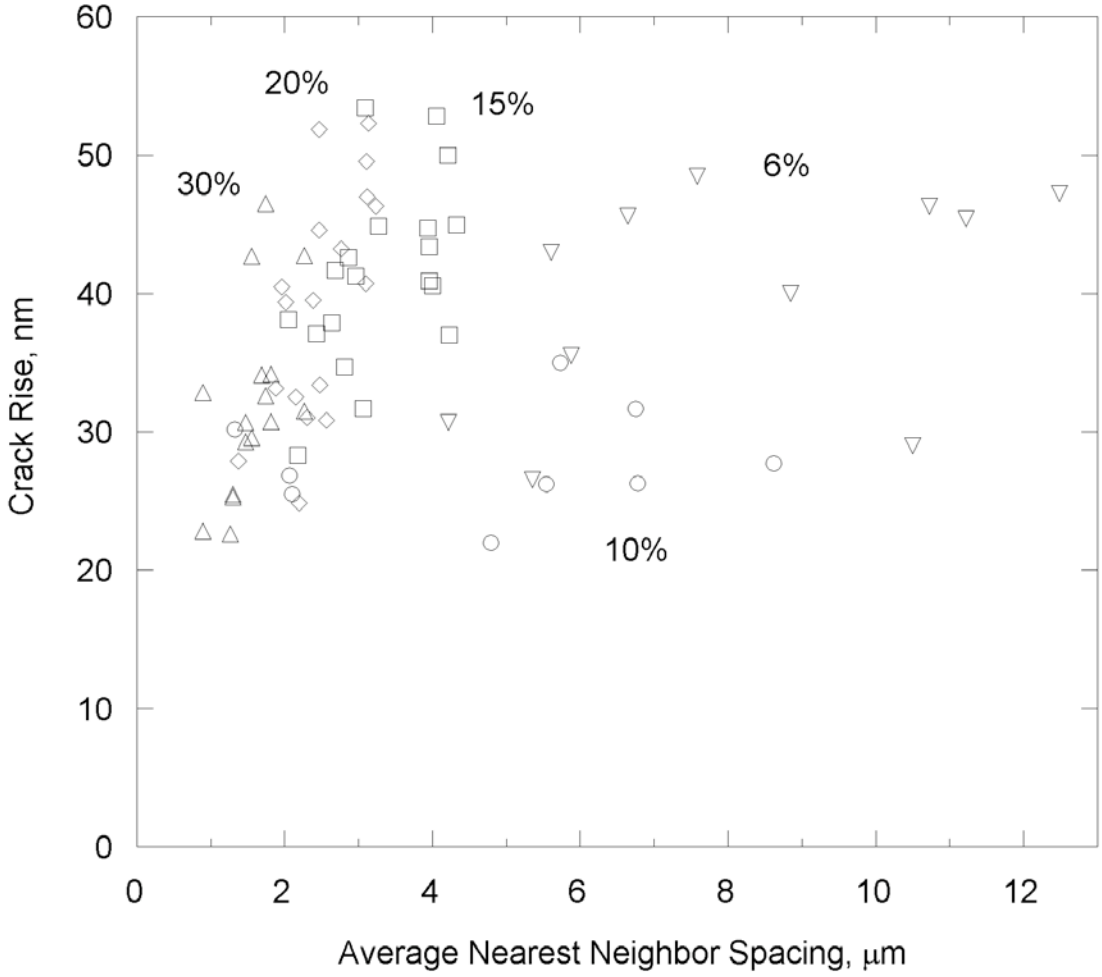

Figure 15b

Figure 15 (a) Crack widths, *w*, and (b) crack rises, *r*, were experimentally measured when possible from the molds of strained specimen and are plotted against the average nearest neighbor crack spacing, *L*, for 6% (∇), 10% (○),15% (□), 20% (◊), and 30% (Δ) applied strain.

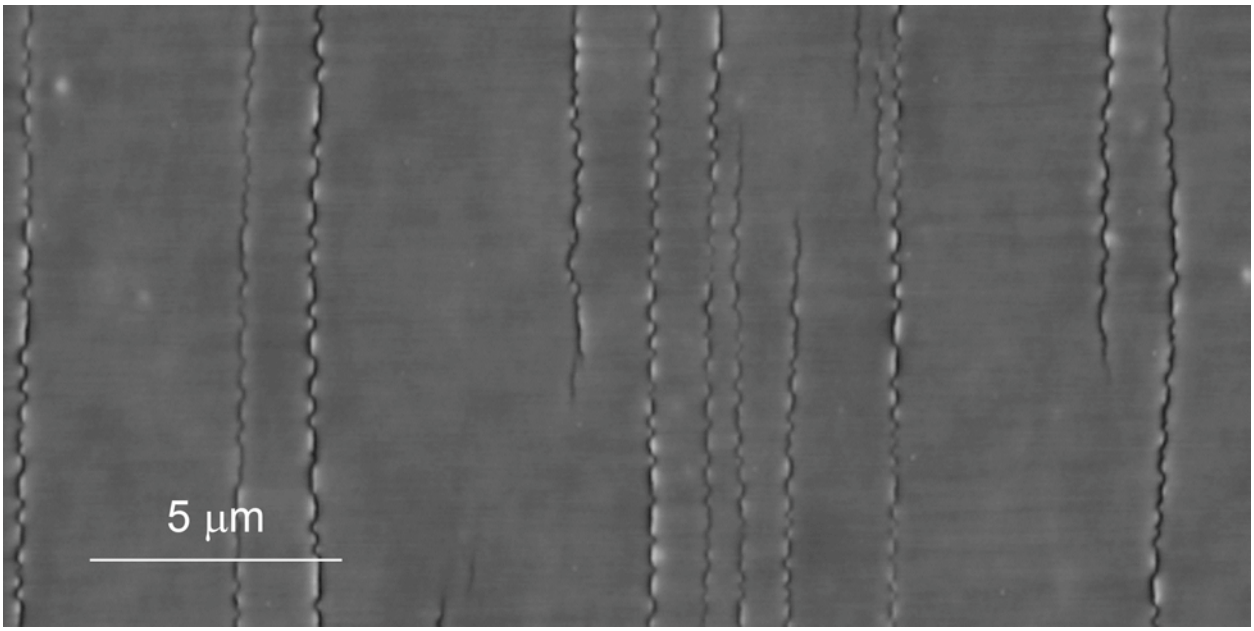

Figure 16 These healed relaxed cracks are on the surface of a relaxed specimen which had been strained to 20%. The cracks collapse due to surface forces acting on the crack faces. Tension induced at the edges of the cracks causes the appearance of buckling. The wavelength of the buckled edge is consistent with the buckling wavelength on the molds of the strained cracks.

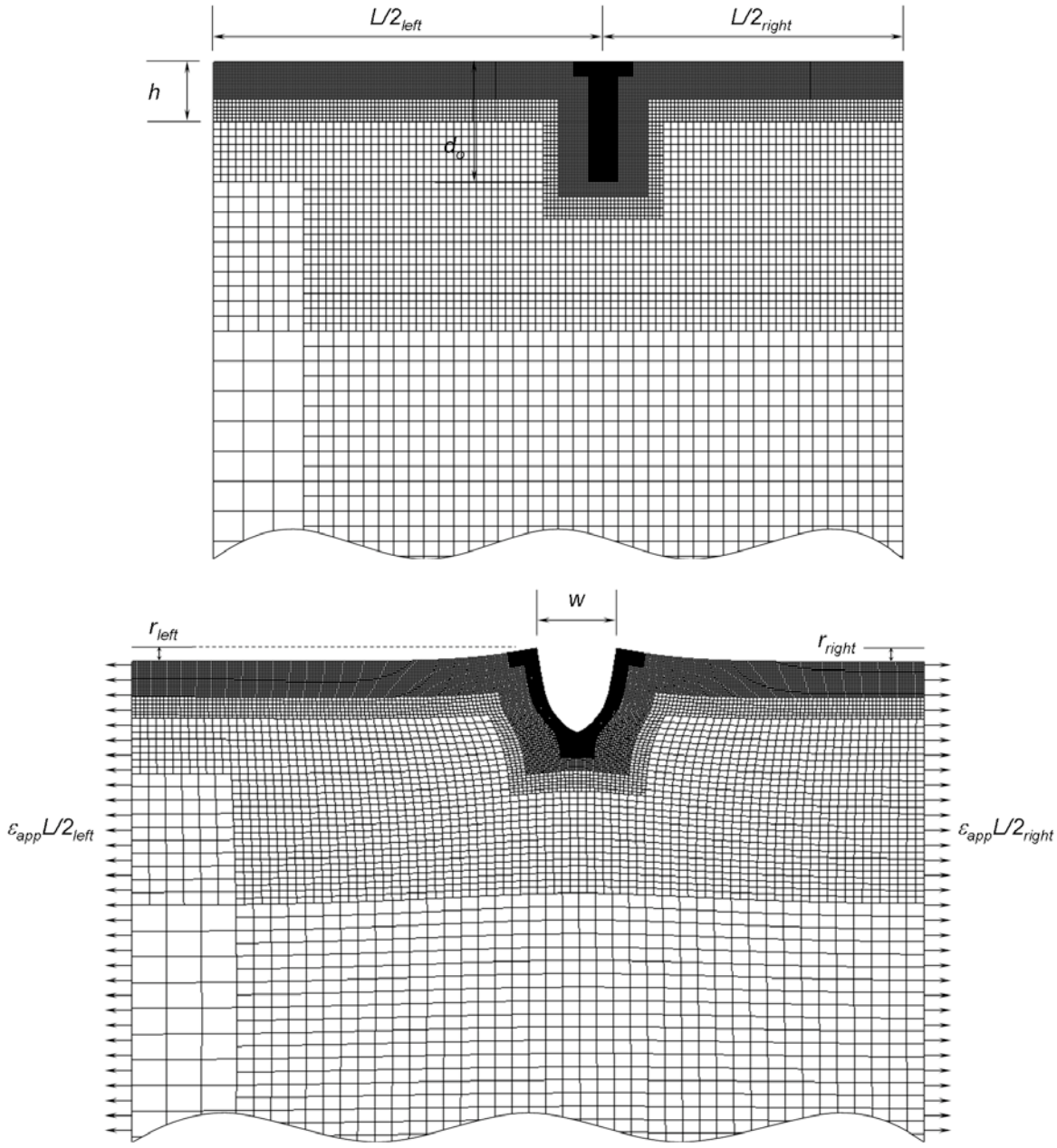

Figure 17 Finite-element mesh used for fitting the width and rise of the cracks to both find the depth of penetration of the cracks and to estimate the average toughness of the surface-modified layer. The lateral dimension on either side of the crack is L/2 for the appropriate crack spacing being modeled. The crack depth can be fixed to anywhere in the region marked d_o. Using the average spacing approach, only half of the crack is modeled and the appropriate periodic boundary condition is applied at the plane corresponding to the crack face.